Regional Stratigraphic Architecture of the Spathian Deposits in Western Canada – Implications for the Montney Resource Play

Tristan Euzen, Thomas F. Moslow, Vincent Crombez, Sébastien Rohais

Regional Stratigraphic Architecture of the Spathian Deposits in Western Canada – Implications for the Montney Resource Play

Authors:

Tristan Euzen, IFP Technologies (Canada) Inc

Thomas F. Moslow, Moslow Geoscience Consulting and Progress Energy Canada Ltd.

Vincent Crombez, IFP Energies nouvelles

Sébastian Rohais, IFP Energies nouvelles

ABSTRACT

Thick Spathian deposits of the Lower Triassic Montney formation are preserved in northeastern British Columbia and west-central Alberta, where they hold massive amounts of unconventional resources. Understanding the internal architecture of these marine deposits at basin-scale can provide a framework to better predict the distribution of source-rocks, reservoirs and seals within this petroleum system and to investigate their control on hydrocarbon generation and migration pathways. Ultimately, this high resolution stratigraphic framework can be used to investigate the impact of geological heterogeneities on well performance at the regional scale.

In northeastern British Columbia, the Spathian deposits consist mainly of offshore and offshore transition sediments forming a wedge prograding from northeast to southwest. This wedge is punctuated by major marine flooding surfaces bounding parasequence sets that can be correlated regionally owing to their characteristic gamma ray logs signature and to the high density of well and core control. The regional correlation of these parasequence sets, based on over 1,450 wells, reveals well-defined clinoform morphologies characterized by topset, foreset and bottomset geometries along a proximal-distal depositional profile. The facies analysis and the characteristic dimensions of these morphologies are consistent with deposition in a predominantly siliciclastic shoreface to shelf setting and marks a significant contrast to the ramp setting of hybrid clastic-carbonate lithologies which prevailed during the Griesbachian to Smithian. The stratigraphic architecture is analogous to “subaqueous shelf-prism clinoforms” that have been described on numerous present-day and ancient continental shelves. Subaqueous shelf-prism clinoforms typically display a

sigmoidal shape in the dip direction and along-shore-elongated depositional thick in plan-view. This geometry results from the interaction of clastic sediment input with shelf hydrodynamic processes such as storm generated waves and sediment gravity flows as well as nearshore and offshore bottom currents. Consequently, the topset, foreset and bottomset of these clinoforms are characterized by different depositional facies that can be predicted and mapped at basin-scale, over hundreds of kilometers.

In the Spathian depositional system of western Canada, clinoform bottomset facies are mainly a product of suspension deposition, hemipelagic sedimentation and mineral precipitation. These facies form the main source-rock intervals within the Montney Formation, due to anoxic conditions and lower sedimentation rates resulting in better preservation of organic matter. Clinoform foresets result from traction transport processes of coarser siliciclastics and higher sedimentation rates, forming thick, mostly organic-lean intervals with better reservoir quality. Foreset deposits form the thickest part of the Spathian parasequence sets and are the main targets of horizontal drilling and multistage fracturing. Clinoform topsets mainly consist of shoreface to offshore transition deposits and are poorly preserved due to the erosion under the top Montney unconformity. The distribution of the depositional thick in map view and along a strike-oriented regional cross-section suggest that these deposits were influenced by major structural elements at basin scale. The regional flooding surfaces bounding the parasequence sets might form extensive permeability barriers that potentially control up-dip migration of hydrocarbons within the Montney petroleum system.

INTRODUCTION

The Lower Triassic Montney Formation of western Canada forms a thick hybrid clastic-carbonate sediment wedge prograding from northeast to the southwest, in Alberta and British Columbia. This formation has been the target of oil and gas exploration and production for over 60 years. Until the 1980's, oil was exploited from conventional reservoirs in bioclastic and siliciclastic shoreline successions of the eastern, proximal part of the depositional system. In the 1990's, natural gas and liquids from turbiditic tight reservoirs were exploited further west into the Deep Basin of west-central Alberta, using vertical wells and hydraulic fracturing. The stratigraphic architecture and the paleogeographic reconstruction of the Montney Formation were mostly developed based on the analysis of the Induan and Lower Olenekian aged deposits containing these shallow marine and turbiditic facies (Davies et al., 1997; Moslow and Davies, 1997; Embry, 1997; Zonneveld et al., 2011). With the recent development of the unconventional reservoirs of the Montney Formation, through horizontal drilling and multistage fracturing, a wealth of new data have been made available in the Upper Olenekien (Spathian Substage) deposits of northeastern British Columbia. The objective of this paper is to illustrate the high-resolution sequence stratigraphy and internal architecture of the Spathian deposits of the Montney Formation at basin scale.

The Montney Formation is subdivided into three third-order sequences which correspond respectively to the Griesbachian-Dienerian, the Smithian and the Spathian Triassic substages (**Fig. 1**; Embry and Gibson, 1995; Davies et al., 1997; Golding et al., 2014; Crombez et al., 2016a and 2016b; Davies and Hume, 2016; Moslow et al., 2016,

Henderson and Schoepfer, 2017). Although several conodont zones were identified within these third-order sequences, published biostratigraphic data do not allow for defining higher resolution units at a regional scale (Gibson and Barclay, 1989; Orchard and Tozer, 1997; Davies et al., 1997; Orchard and Zonneveld, 2009; Golding et al., 2011; Golding et al., 2014; Henderson and Schoepfer, 2017). However, based on well log correlations, internal clinoform morphologies have long been recognized within the Griesbachian-Dienerian and Smithian sequences (Davies et al. 1997, Wilson et al. 2012, Davies and Hume 2016), and more recently within the Spathian sequence (Dixon, 2009; Lynch and Stasiuk, 2011; Wilson et al., 2012; Wood, 2013, Euzen et al 2017). In the Spathian deposits, these clinoforms form internal packages separated by extensive flooding surfaces that can be correlated regionally, owing to their characteristic gamma ray log signature and to the very high density of well control. However, to our knowledge, basin-scale correlation and mapping of these internal units have not been published. This paper aims at filling this gap by presenting the results of basin-scale correlation and mapping of the Spathian internal architecture, based on over 1,450 wells. The implications of this work on the paleogeographic reconstruction and sequence stratigraphic interpretation of the Spathian deposits are discussed. The cross-sectional morphology and plan-view geometry of the Spathian internal units, as well as the facies partitioning within them, have a direct impact on the distribution of source rocks, reservoirs and seals within the unconventional Montney play.

DATA AND METHOD

The interpretation presented in this work is based on the correlation of over 1,450 wells using the gamma ray logs and detailed sedimentologic descriptions of 6 full - diameter cores through the entire Spathian succession (**Fig. 2**).

Our well database contains over 1,450 wells with a gamma ray log over the complete Spathian section and covers an area of about 50,000 square kms, from the Elmworth Field of Alberta in the southeast to the Caribou Field of British Columbia in the northwest. The study area extends from the erosional pinchout of the Spathian deposits to the east and south, to the Cordillera deformation front or slightly beyond to the west and southwest **(Fig. 2)**. Well to well correlation was performed by constructing tens of dip-oriented cross-sections throughout the study area from the updip topset to the downdip bottomset of clinoforms where preserved. Due to variations in calibration and vintage of gamma ray logs, the API scale was set individually for each well, to maximize the variability and magnify high frequency patterns of cyclicity. The unconformable surface at the base of the Spathian substage and the Montney-Doig boundary (base of the Doig 'Phosphatic Member') were both used alternatively as a datum to verify the consistency of correlations.

The sedimentological expression of major flooding surfaces, the lateral facies variations along the depositional profile and the vertical facies evolution of the Spathian succession were investigated using selected core descriptions from 6 wells (400 m of cumulative thickness). The thickness of the parasequence sets bounded by the flooding surfaces was mapped throughout the basin and discussed in terms of reservoir and source-rock distribution, as well as structural controls on sedimentation.

CORE-LOG CALIBRATION OF MAJOR FLOODING SURFACES

In the Spathian sequence, the gamma ray log signature is strongly influenced by the uranium concentration, as observed in spectral gamma ray data (**Fig. 3**). Uranium precipitation in sediments is influenced by redox conditions as well as by the abundance of reactive organic matter (Tribovillard et al., 2006). Uranium is also concentrated in phosphate enriched layers, often associated with condensed intervals with multiple reworking/winnowing episodes (Li and Schieber 2015). As observed in full-diameter cores within the Spathian interval, flooding surfaces are associated with massive-appearing bituminous siltstone with higher organic content and occasionally with pebbly siltstone phosphatic lags (**Fig. 3 and 4**). These flooding events have a regional extent and can therefore be correlated across the basin over several hundreds of km, based on the gamma ray log signature. However, correlating these flooding surfaces with a good level of confidence requires a high density of well control especially where the Spathian units become more condensed in the downdip (bottomset) and updip (topset) directions. In those areas, the distance between wells used for the correlation was kept between 1 and 3 km where possible.

INTERNAL ARCHITECTURE OF THE SPATHIAN SUBSTAGE

The Spathian deposits correspond to the third and youngest 3rd-order sequence of the Montney Formation. This sequence is bounded below by a sequence boundary corresponding to the Smithian-Spathian unconformity and above by a coplanar sequence boundary and transgressive surface of erosion separating the Montney Formation from the overlying Doig 'Phosphatic Member' of the Doig Formation (Golding et al., 2015; Crombez, 2016). Recent work demonstrates that an

unconformity-bounded Early Anisian unit thickening downdip to the west, informally named 'Anisian Wedge', is present between the Montney and Doig Formations (Zonneveld et al., 2016; Furlong et al., 2017; Furlong et al. a and b, this volume).

PARASEQUENCE SETS AND MORPHOLOGY OF THE CLINOFORMS

Clinoforms are seaward dipping stratal surfaces commonly observed on seismic data in present-day and ancient coastal, shelf and continental margin depositional systems (Nittrouer et al. 1996; Hampson 2010, Helland-Hansen el al, 2012; Patruno et al. 2015). The proximal-distal cross-sectional morphology of a clinoform typically consists of gently basinward-dipping topset and bottomset separated by a steeper foreset, with slope changes occurring through upper and lower rollover points respectively up-dip and down-dip of the foreset. Patruno et al. (2015) analyzed a large morphological dataset of present-day and ancient clinoform systems, and defined four main type of clinoforms associated with different scales and controlling processes. In subaerial delta clinoforms, the upper rollover point corresponds to the shoreline, whereas in subaqueous delta or shelf-prism clinoforms the transition between the topset and the foreset occurs at 10's to 100's of meters in water depth. At an even larger scale, continental margin clinoforms are associated with the continental slope, with water depth of the upper rollover point typically occurring at depths greater than 1000 meters (Patruno et al., 2015). Analyzing the characteristic dimensions of the Spathian clinoform morphologies observed in the Montney Formation and the depositional facies associated with them, can help to better understand the physiography of the basin at the time of deposition.

Figure 5 illustrates the internal architecture of Spathian deposits along six dip-oriented regional cross-sections, from the Dawson area to the south to the Caribou area to the north. The datum for these cross-section was set at the base of the Doig Formation 'Phosphatic Member'. Seven regionally correlatable internal units were defined within the Spathian sequence (**Fig. 5**). These units are interpreted as parasequence sets because they contain several smaller-scale parasequences, bounded by major marine flooding surfaces and are themselves contained within depositional sequence systems tracts (Catuneanu et al., 2009). They have been numbered M3-1 through M3-7, the first number corresponding to the sequence (third-order sequence 3 of the Montney Formation *sensu* Crombez, 2016) and the second number corresponding to the parasequence set from oldest to youngest (bottom to top). Some of the uppermost deposits of the top unit (M3-7) have been identified as part of the 'Anisian Wedge' from core data (Furlong et al 2017) and are therefore of Anisian age (**see Fig. 1**). The 'Anisian Wedge' was not mapped in this study, but it is the focus of two papers within the present volume (Furlong et al. a and b, this volume).

The flooding surfaces bounding the Spathian parasequence sets clearly define sigmoidal clinoform morphologies (Euzen et al., 2017) along dip-oriented cross-sections **(see Fig. 5C, 5E and 5F)**. These morphologies are only fully preserved in the lower part of the Spathian succession (units M3-1 to M3-4), as the proximal part of the overlying units (M3-5 to M3-7) have been eroded beneath the basal Doig unconformity. The geometry of the lower Spathian clinoforms can be observed from the low angle topset in the northeast, through the paleo-seaward dipping foreset where the parasequence sets thicken, down to the subparallel bottomset. The

bottomset interval is characterized by a spiky gamma ray log signature interpreted to be due to the condensation of multiple cycles in a starved offshore setting. This high cyclicity may have resulted from changes in the relative balance between bottom water oxygenation and sedimentation rate. As observed in core, bottomset facies are highly bituminous to kerogenous, phosphatic siltstones (high gamma ray values) interbedded with calcareous dolosiltstones of hemipelagic origin (low gamma ray values). The foreset region is characterized by a steeper slope and a depositional thick of parasequence sets that thin basinward and landward. In many places, the thinning of individual parasequences is clearly associated with a vertical contraction of the GR log pattern, suggesting that the change of thickness results from variations of the sedimentation rate along the depositional profile (see the lateral variation of gamma ray signature in unit M3-2 along the cross-section C of Fig. 5).

VERTICAL AND LATERAL FACIES EVOLUTION

The sedimentological description and depositional interpretation of a set of selected cores were used to investigate the vertical and lateral facies variability within the Spathian parasequence sets and along the depositional profile from the topset to the bottomset of clinoforms. There are four principal facies recognized from the Spathian interval of the study area. Their principal sedimentary characteristics and interpreted environments of deposition are illustrated in **Fig. 6 and 7**. Observed lithologies vary from siliciclastic to phosphatic in composition. Based primarily on physical and biogenic sedimentary structures, processes of deposition are inferred for each facies providing the basis for environmental interpretation. All four facies are interpreted to have been the product of storm, wave and/or suspension settling processes of deposition in lower shoreface through offshore environments of deposition as part of

an inner continental shelf, as opposed to ramp, profile (Moslow et al, 2016) **(Fig. 8)**. Siliciclastic facies are predominantly bituminous siltstone to silty very-fine grained sandstone with the former lithology being far more common. In more distal environmental settings, bituminous matrix increases and grain size decreases. Conversely, sedimentary facies deposited in a more proximal position on the shoreface-shelf profile have a less bituminous matrix, coarser grain size and higher net to gross of coarse siltstone and very- fine grained sandstone to total bulk volume textural composition.

Lower shoreface facies are observed in core as sparsely to moderately burrowed, occasionally cryptobioturbated, planar laminated, wavy bedded fine to coarse-grained siltstone, interbedded with very fine-grained silty sandstone. Macro-scale burrow traces include diminutive forms of Bergaueria, Palaeophycus, Lingulichnus and Skolithos. Normally-graded, sharp-based planar-laminated silty sandstone beds with burrowed tops and varying in thickness from 3-5cm are interpreted as tempestites (**Fig. 6A**). Offshore transition facies are observed as parallel-laminated to lenticular-bedded, burrowed to cryptobioturbated fine to coarse-grained siltstone (**Fig. 6B**). Trace fossils occur either as diminutive forms within a distal Cruziana assemblage with low to moderate diversity, interpreted as part of the proximal offshore transition environment, or as cryptobioturbation, interpreted as being characteristic of the distal offshore transition environment. Offshore facies are highly bituminous to occasionally kerogenous, massive-appearing to faintly parallel-laminated, fine to coarse-grained siltstone with frequent phosphatic lenses and laminae (**Fig. 6C**). Phosphatic clasts or nodules are sporadically observed in proximal and distal offshore transition deposits as well. Calcareous, calcispheric dolosiltstones, interpreted as

241 hemipelagite deposits, form 5 to 30 cm thick inversely graded beds and are observed
242 within the bottomset and foreset areas of the clinoforms, throughout the Spathian
243 succession (**Fig. 6D**).

244 The topset clinoform setting is dominated by proximal offshore transition to lower
245 shoreface deposits, whereas the foreset setting is dominated by distal offshore
246 transition facies (**Fig. 7**). The bottomset clinoform setting dominantly consists of
247 bituminous to kerogenous fine to coarse-grained siltstone with phosphatic lenses and
248 laminae deposited in an offshore environment of deposition, and interbedded with
249 hemipelagites. The lateral distribution of sedimentary facies and inferred depositional
250 environments suggest that the upper rollover point of the clinoforms corresponds
251 approximately to the limits between proximal and distal offshore transition
252 (corresponding to the mean storm wave base), whereas the lower rollover point
253 would mark the change from offshore transition to offshore (basinward influence of
254 storm waves: **Fig. 8**). These observations support the interpretation of Montney
255 Spathian deposition on a shoreface to inner shelf setting comparable to the
256 morphology of muddy subaqueous deltas or shelf-prism clinoforms (Patruno et al,
257 2015). In this setting and with respect to the Montney, the transition between the
258 topset and the foreset of clinoforms does not correspond to a shoreline break but is
259 instead associated with pre-existing (Smithian) subaqueous topography and a change
260 in hydrodynamic processes of deposition and concomitant increase in sedimentation
261 rate.

262 In the foreset area, the vertical stacking pattern of sedimentary facies reflects an
263 overall progradation throughout the Spathian, with an upward increasing proportion
264 of proximal offshore transition or lower shoreface deposits, depending on location in

the basin (**Figure 9**). This progradation is punctuated by flooding surfaces demarcated by a rapid and sustained shift in water deepening as observed in core by an immediately overlying facies change to a relatively thick occurrence of offshore facies composed of massive-appearing bituminous siltstones, occasionally associated with calcispheric dolosiltstone of hemipelagic origin. However, calcispheric dolosiltstone intervals are observed throughout the Spathian succession (see **Fig. 4**) and are not necessarily associated with the flooding surfaces bounding parasequence sets (highlighted by purple arrows on **Fig. 9**). Calcispheres in the Montney formation may be the product of deposition associated with algal blooms (Chau and Henderson, 2010) or possibly dinoflagellate blooms (G. Davies, 2015, pers. comm.; Moslow et al, 2016). Given the frequency of these dolosiltstone beds (46 throughout the Spathian succession in well c-65-F/94-B-08 for example) and the duration of the Spathian interval (ca. 1.5 My; Henderson and Schoepfer, 2017), these intervals might reflect obliquity and/or precession Milankovitch cycles (Henderson and Schoepfer, 2017).

In the topset area of the proximal part of the basin, the vertical stacking of offshore sediments on top of shoreface deposits suggests a downlap surface (see well 04-16-078-12W6, **Fig. 9**).

MAPPING OF THE PARASEQUENCE SETS

Figure 10 shows the isopach maps of the parasequence sets M3-1 through M3-4 at regional scale. These four lower Spathian units were selected to illustrate the depositional morphology of the clinoforms, because they were well preserved as opposed to the overlying units M3-5 to M3-7, that were extensively eroded under the top Montney unconformity, in the eastern proximal part of the study area. These

maps display the depositional thick of each unit (thickness>10m), that corresponds to the foreset area of the clinoforms. The thickness of the parasequence sets in the topset and bottomset areas typically is around 10m or less and increases up to over 60m in foreset areas. The width of the foreset area corresponds to the distance between the upper and lower rollover points, and varies between 30 and 50km in the dip direction. The thickness and the orientation of the foreset depositional thicks also vary along strike as illustrated by the isopach maps (**Fig. 10**). Each unit presents two or three depositional thick separated by thinner areas. A 330 km-long strike-oriented NW-SE cross-section of the Montney Formation (**Fig. 11**), suggests that major structural elements may have influenced these thickness variations (Berger et al., 2008). The thinning of the Montney Formation over the Fort St. John Graben might indicate that this structure was inverted during the deposition of the Montney Formation. Another thinning of the Montney Formation occurs across a major fault bounding the Laurier Embayment (Berger et al., 2008). Thinner areas generally correspond to transition zones where the orientation of the clinoform changes. These changes of orientation and thickness along strike suggest a regional structural control on sedimentation and possibly the occurrence of tectonically-controlled localized sediment sources.

These regional structural discontinuities may have influenced subsidence variations across the basin and potentially controlled the location of sedimentary entry points into the basin. Differential subsidence across the basin may be due to tectonic movements and/or to differential compaction due to variable thickness of the pre-Triassic sediment cover on top the basement (Rohais et al., this volume). Such a structural control on sediment sources and transport directions have previously been

312 suggested in the Montney Formation (Davies et al., 1997; Moslow and Davies, 1997;
313 Zonneveld and Moslow, 2014; Davies and Hume, 2016).

314 A compensation effect between units 3-1 and 3-2 due to depositional paleorelief is
315 also suggested by a switch in the position of the thick areas (**Fig. 10**).

316 **PALEOGEOGRAPHIC RECONSTRUCTION**

317 Reconstructing the paleogeography of the Montney Formation during Spathian time is
318 impeded by the non-preservation of the coeval shoreline and nearshore deposits that
319 were eroded under the top Montney/base Doig unconformities, in the eastern
320 proximal part of the basin. However, analyzing the dimensions and depositional
321 environment of the Spathian clinoforms and comparing them to ancient or recent
322 analogues, can provide useful information to better understand the physiography of
323 the basin at the time of deposition. The facies analysis of the Spathian clinoforms
324 suggests that the upper rollover point between the topset and the foreset occurs
325 within or close to the mean storm-weather wave base, typically at 15 to 40 m of
326 water depth (Coe et al 2006).

327 The non-preservation of Spathian coastal deposits implies that the coastline was
328 located eastward from the present-day subcrop edge of the Spathian. Based on a
329 comparative analysis of morphological parameters from over a hundred clinoform
330 systems, Partuno et al (2015) highlighted a strong correlation between the distance
331 from the shoreline to the clinoform toe point (Hd) and the width of the foreset (Fd)
332 (see Fig. 5 and Fig. 14D in Patruno et al., 2015). The comparison of the width of the
333 foreset mapped in the Spathian deposits (30 to 50 km, see **figure 10**) with subaqueous

clinofrom analogues, suggests a distance between the shoreline and the clinoform toeset (Hd) in the range of 90 to 150 km.

Based on the above considerations, **Figure 12** illustrates a schematic paleogeographic reconstruction of the lower Spathian depositional system. On this map, the bottomset offshore region in dark blue represents an organic-rich area during the deposition of the lower units of the Spathian (Crombez et al., 2016b). The foreset, offshore transition to offshore region in medium blue corresponds to the area where thick bioturbated siltstone reservoirs were deposited during the Lower Spathian (Moslow et al., 2016). The topset, offshore transition to lower shoreface region corresponds to the area where the Spathian deposits thin both depositionally and erosionally, preventing the development of thick Spathian reservoirs.

STRATIGRAPHIC ARCHITECTURE OF THE SPATHIAN DEPOSITS

A sequence stratigraphic interpretation of the Montney Spathian succession was proposed by Davies and Hume (2016), where a lowstand wedge onlaps on the basal sequence boundary just eastward of the Alberta-BC border, and a highstand systems tract (HST), corresponding to the "Lower Doig Siltstone" in Alberta, progrades westward and downlaps onto the lowstand systems tract (LST). The lowstand wegde thickens to the west, but their schematic cross-section does not extend beyond Range 17W6 (see Fig. 2 in Davies and Hume, 2016).

The correlation and mapping of the present study extends over about a hundred kilometer further downdip into the basin and shows that the lower Spathian parasequence sets becomes thinner and organic-rich westwards in the bottomsets of the clinoforms. **Figure 13** illustrates the stratigraphic architecture of the Spathian

parasequence sets within the broader context of the Montney Formation, along five dip-oriented schematic regional cross-sections throughout the basin, from Dawson to Beg areas (datum at the base of the Doig Fm.). These cross-sections highlight the onlap of the lower Spathian units to the west on the Smithian-Spathian sequence boundary (Montney Sequence 3). The facies stacking patterns from core descriptions (Moslow, 2016) and the overall aggradation of units M3-1 and M3-2 suggest that the top of unit M3-2 might correspond to a 3rd order maximum flooding surface. Alternatively, the apparent truncation of the units M3-3 and M3-4 to the west along the Dawson cross-section (see **Fig. 13**) could tentatively be interpreted as associated with a co-planar transgressive and maximum flooding surfaces, with internal downlap onto this surface within the overlying unit M3-5. The vertical stacking of the of offshore deposits on top of shoreface deposits in the proximal well 04-16-078-12W6 (see **Fig. 9**) might correspond to this downlap surface.

However, identifying this surface recording the maximum landward migration of the shoreline, remains challenging because the coastal deposits to the east were not preserved due to erosion under the basal Doig unconformity. A more detailed analysis with additional core control along dip-oriented regional cross-sections would be required to clearly identify at basin-scale the downlap surface corresponding to the third-order maximum flooding surface of Montney sequence3.

Clinoform morphologies are well developed along the Dawson and Groundbirch cross-section of **Fig 13**, but tend to be less well defined in the north, especially along the northernmost cross-section in the Beg area. This may be related to the influence of an additional sediment source to the north or northwest, perpendicular to this cross-section. Another striking feature of the northern cross-sections on **Fig. 13** is the

overall thinning of the Spathian succession to the far west. This may be an artefact created by the use a datum that was a basinward dipping surface at the time of deposition. Alternatively, it might be interpreted as resulting from uplift and erosion to the west, below the base Doig unconformity (Rohais et al., 2017; this volume).

IMPLICATIONS FOR THE MONTNEY PLAY

The reconstruction of the internal architecture of the Spathian succession and the mapping of parasequence sets provide a framework to better predict the distribution of source-rock and reservoir intervals at regional scale in the upper part of the Montney play in northeastern British Columbia and west-central Alberta.

The bottomsets of the clinoforms identified in the lower part of the Spathian succession correspond to condensed intervals with present day TOC values typically up to 4-7 wt% (Crombez et al., 2016b). The bottomset region (**Fig. 12**) is in the deep overmature part of the basin, preventing the characterization of this source-rock in its early stage of maturation. Assuming an initial hydrogen index of 450 mg HC/g TOC, the initial TOC of these organic-rich deposits would have been in the range of 5-10 wt% (Crombez et al., 2016b). Together with the Doig 'Phosphatic Member', these offshore Spathian deposits are potentially a significant source of hydrocarbons for the distal Montney play.

The foreset of the clinoforms up-dip from the offshore region are characterized by thicker offshore transition facies of burrowed, crypto-bioturbated, parallel laminated to lenticular bedded fine- to coarse-grained bituminous siltstone. The macro-scale burrowing and crypto-bioturbation in these foreset siltstones preserve intergranular porosity by inhibiting the precipitation of calcite cement and enhancing vertical

permeability (Moslow et al., 2014). The upper Spathian to lower Anisian units prograde over the offshore region of the lower Spathian units, superimposing higher net to gross offshore transition deposits on top of organic-rich lower Spathian organic-rich siltstones. These thick reservoir intervals are stratigraphically located between two source-rock intervals, with the Spathian bottomset offshore deposits below and the Doig 'Phosphatic Member' above them. The bottomsets of these upper Spathian clinoforms probably consisted of organic-rich sediments deposited further west, but that are now part of the Canadian Cordillera.

The extensive flooding surfaces bounding the parasequence sets are associated regionally continuous metric to plurimetric massive siltstone layers with lower permeability (Euzen et al., 2015; 2017). These intervals may have hindered crossflow between the Spathian parasequence sets and controlled up-dip fluid migration during the burial history of the Montney Formation (Wood, 2013). The reservoir quality and geomechanical properties of the foreset bioturbated siltstone may also vary from one unit to the other, due to changes in sediment source dynamics and/or paleo-ecological parameters through time. Chemostratigraphic differences between the Spathian parasequence sets support this hypothesis (Chemostrat unpublished report, 2011). Consequently, each parasequence set may have unique production characteristics associated with specific reservoir properties and migration history.

CONCLUSIONS

Thanks to a wealth of new well data resulting from the recent development of the distal unconventional part of the Montney play, it is now possible to decipher the internal stratigraphic architecture of the Spathian deposits at basin scale. Based on over 1,450 wells, this paper presents the correlation of seven parasequence sets and mapping of four of them that were preserved from the topset to the bottomset of the clinoforms. The regional distribution of these internal units, combined with core descriptions and facies analysis, provide the basis for the reconstruction of the stratigraphic architecture and paleogeography of the Montney Formation during Spathian time. Implications for the Montney play are discussed in terms of source-rock, reservoir and seal distributions.

The parasequence sets of the Spathian succession are bounded by extensive flooding surfaces that clearly define clinoform morphologies. The dimensions of these depositional geometries compared with present day and ancient analogues, as well as the facies analysis from core descriptions, suggest that they correspond to subaqueous delta or shelf-prism clinoforms. The foreset of these clinoforms form depositional thicks dominated by bioturbated siltstone deposited in offshore transition settings. These foresets thin downdip to form organic-rich bottomsets deposited in the offshore environment. The lateral, along-strike variations of thickness and orientation of the depositional thick of parasequence sets suggest differential subsidence across the basin, associated with syn-sedimentary tectonic movements and/or differential compaction of the pre-Triassic sedimentary cover. Major structural elements such as the Fort St. John Graben and the Laurier

Embayment may also have controlled the location of sedimentary entry points into the basin.

Our model provides a stratigraphic framework to better predict the distribution of source-rocks and reservoirs in the Montney Spathian deposits. Bottomsets of the Spathian clinoforms are good potential source rocks for hydrocarbons in the Montney play and were deposited in the western deep and now overmature part of the basin. Individual parasequence sets may have specific reservoir characteristics resulting from variations in sediment source dynamics and/or paleo-ecological conditions. Furthermore, the extensive flooding surfaces bounding the parasequence sets may have acted as regional permeability barriers and influenced the distribution of fluids within the Spathian deposits. These depositional heterogeneities can therefore result in variable production characteristics between different parasequence sets. To validate this model and better understand the depositional controls on Montney productivity at basin-scale, a statistical analysis of normalized well production within the stratigraphic framework developed in this work is now possible.

ACKNOWLEDGEMENTS

The authors would like to acknowledge Progress Energy Canada Ltd. for authorizing the use and publication of the core descriptions used in this manuscript. We also thank Brad Hayes, Graham Davies and Mark Caplan for their constructive comments and suggestions that helped improve the manuscript.

REFERENCES

Berger, Z., Boast, M., and Mushayandebvu, M. 2008. The contribution of Integreated HRAM Studies to Exploration and Exploitation of Unconventional Plays in North America. Reservoir, 35(10), 42–47.

Catuneanu, O., Abreu, V., Bhattacharya, J.P., Blum, M.D., Dalrymple, R.W., Eriksson, P.G., Fielding, C.R., Fisher, W.L., Galloway, W.E., Gibling, M.R., Giles, K.A., Holbrook, J.M., Jordan, R., Kendall, C.G.S.C., Macurda, B., Martinsen, O.J., Miall, A.D., Neal, J.E., Nummedal, D., Pomar, L., Posamentier, H.W., Pratt, B.R., Sarg, J.F., Shanley, K.W., Steel, R.J., Strasser, A., Tucker, M.E. and Winker, C. 2009. Towards the standardization of sequence stratigraphy. Earth-Science Reviews, v. 92, p. 1–33. doi:10.1016/j.earscirev.2008.10.003

Chau, Y.P. and Henderson, C.M. 2010. The Lower Triassic Sulphur Mountain Formation, Mount Crum Section, east-central British Columbia: age, tectonic implications and Montney lithofacies comparisons. abstract, CSPG CSEG CWLS Joint Annual Convention, Calgary, 10-14 May 2010. Available from: http://www.geoconvention.com/archives/2010/0902_GC2010_The_Lower_Triassic_Sulphur_Mountain_Fm.pdf

Coe, A.L., Bosence, D.W.J., Church, K.D., Flint, S.S., Howell, J.A., and Wilson, R.C.L. 2003. The sedimentary record of sea-level change: Cambridge, UK, Cambridge University Press, 288 p.

Crombez, V., Rohais, S., Baudin, F. and Euzen, T. 2016a. Facies, well-log patterns, geometries and sequence stratigraphy of a wave-dominated margin: insight from the Montney Formation (Alberta, British Columbia, Canada). Bulletin of Canadian Petroleum Geology, v. 45, p. 474–505.

Crombez, V., Baudin, F., Rohais, S., Riquier, L., Euzen, T., Pauthier, S., Ducros, M., Caron, B., and Vaisblat, N., 2016b. Basin scale distribution of organic matter in marine fine-grained sedimentary rocks: Insight from sequence stratigraphy and multi-proxies analysis in the Montney and Doig formations, Marine and Petroleum Geology (2016), doi: 10.1016/j.marpetgeo.2016.10.013.

Davies, G, Moslow, T.F. and Sherwin, M.D. 1997. The Lower Triassic Montney Formation, West-Central Alberta. Bulletin of Canadian Petroleum Geology, v. 45, p. 474–505.

Davies, G.R. and Hume, D. 2011. 'Upper' Montney-'lower' Doig: quo vadis?. CSPG CSEG CWLS Join Annual Convention: May 9-11 2011, Calgary, AB. Available from: http://www.geoconvention.com/archives/2011/319-Upper_%20Montney_Lower_Doig.pdf

507 Davies, G.R. and Hume, D. 2016. Lowstand / Slope-Onlap Wedges in the
508 Montney: Stratigraphic and Sequence Framework, Reservoir Significance.
509 CSPG CSEG CWLS Join Annual Convention: March 7-9 2016, Calgary,
510 AB.

511 Dixon, J. 2009. The Lower Triassic Shale member of the Montney Formation in
512 the subsurface of northeast British Columbia; Geological Survey of
513 Canada, Open File 6274.
514 http://ftp.geogratis.gc.ca/pub/nrcan_rncan/publications/ess_sst/248/248223
515 /of_6274.zip

516 Embry, A.F. and Gibson, D.W. 1995. T-R sequence analysis of the Triassic
517 succession of the Western Canada Sedimentary Basin. In: Proceedings of
518 the Oil and Gas Forum '95 - Energy from Sediments. J.S. Bell, T.D. Bird,
519 T.L. Hillier and EL. Greener (eds.). Geological Survey of Canada, Open
520 File 3058, p. 25-32.

521 Embry, A.F. 1997. Global Sequence Boundaries of the Triassic and Their
522 Identification in the Western Canada Sedimentary Basin. Bulletin of
523 Canadian Petroleum Geology, v. 45, p. 415–433.

524 Euzen, T., Everett, B., Power, M., Crombez, V., Rohais, S., Vaisblat, N., &
525 Baudin, F. 2015. Geological Controls on Reservoir Properties of the
526 Montney Formation in Northeastern BC: An integration of sequence
527 stratigraphy, organic geochemistry, quantitative mineralogy and

528 petrophysical analysis. CSPG CSEG CWLS Join Annual Convention: May
529 4-6 2015, Calgary, AB. Available from:
530 http://www.geoconvention.com/archives/2015/201_GC2015_Geological_
531 Controls_on_Reservoir_Properties.pdf

532 Euzen, T., Moslow, T.F., Crombez, V. and Rohais, S. 2017. Basin-scale high-
533 resolution sequence stratigraphy and internal architecture of the Spathian
534 deposits of the Montney Formation in Western Canada (Lower Triassic)..
535 CSPG CSEG CWLS Join Annual Convention: May 15-19 2017, Calgary,
536 AB. Available from:
537 http://www.geoconvention.com/uploads/2017abstracts/099_GC2017_Basi
538 n-scale_high-resolution_sequence_stratigraphy.pdf

539 Feng, W., Chen, Z. and Jiang, C. 2016. Oil and Source Correlations of Triassic
540 Monteney Formation in WCSB : Implication to Shale Gas Resource
541 Potential. CSPG CSEG CWLS Join Annual Convention: March 7-9 2016,
542 Calgary, AB. Available from:
543 http://www.geoconvention.com/archives/2016/083_GC2016_Oil_and_Sou
544 rce_Correlations_of_Triassic_Monteney_Fm_WCSB.pdf

545 Furlong, M., Gingras, M.K. and Zonneveld, J.P. 2017. The 'Anisian Wedge':
546 Insight on the Complexity of the Montney Doig Boundary. CSPG CSEG
547 CWLS Join Annual Convention: May 15-19 2017, Calgary, AB. Available
548 from:

http://www.geoconvention.com/uploads/2017abstracts/122_GC2017_The_Anisian_Wedge-Insight_on_Complexity_of_Montney-Doig_Boundary.pdf

Furlong et al. The Sunset Prairie Formation: Designation of a New Middle Triassic Formation between the Lower Triassic Montney Formation and Middle Triassic Doig Formation in the Western Canada Sedimentary Basin. T. Euzen, T.F. Moslow and M. Caplan, (eds). The Montney Play: Deposition to Development. CSPG Special Volume.

Furlong et al. Sedimentology and Ichnology of the Middle Triassic (Anisian) Sunset Prairie Formation of the Western Canada Sedimentary Basin. T. Euzen, T.F. Moslow and M. Caplan, (eds). The Montney Play: Deposition to Development. CSPG Special Volume.

Gibson, D.W. and Barclay, J.E. 1989. Middle Absaroka Sequence - the Triassic stable craton. In: Western Canada Sedimentary Basin - a Case History. B.D. Ricketts (ed.). Canadian Society of Petroleum Geologists, Special Publication No. 30, p. 219-232.

Golding, M.L., Zonneveld, J-P., Or chard, M.J., Ferri, F. and Mortensen, J.K. 2011: Stratigraphic correlation and sedimentary provenance of Triassic natural gas–bearing rocks in northeastern British Columbia (NTS 094B): correlation of outcrop to the subsurface; in Geoscience BC Summary of Activities 2010, Geoscience BC, Report 2011-1, p. 229–238.

http://www.geosciencebc.com/i/pdf/SummaryofActivities2010/SoA2010_Golding_etal.pdf

Golding, M.L., Orchard, M.J., Zonneveld, J.-P., Henderson, C.M. and Dunn, L. 2014. An exceptional record of the sedimentology and biostratigraphy of the Montney and Doig formations in British Columbia. Bulletin of Canadian Petroleum Geology, v. 62, p. 157–176.

Golding, M.L., Orchard, M.J., Zonneveld, J.-P. and Wilson, N.S.F. 2015. Determining the age and depositional model of the Doig Phosphate Zone in northeastern British Columbia using conodont biostratigraphy. Bulletin of Canadian Petroleum Geology, v. 63, p. 143–170.

Hampson, G. J. 2010. Sediment dispersal and quantitative stratigraphic architecture across an ancient shelf. Sedimentology, 57(1), 96–141. http://doi.org/10.1111/j.1365-3091.2009.01093.x

Helland-Hansen, W., Steel, R.J., & Somme, T.O. 2012. Shelf genesis revisited. Journal of Sedimentary Research, 82(3), 133–148.

Henderson, M.H. and Schoepfer, S. High-Resolution Biostratigraphic and XRF-Geochemical Correlation of the Montney Formation, NEBC. CSPG CSEG CWLS Join Annual Convention: May 15-19 2017, Calgary, AB. Available from: http://www.geoconvention.com/uploads/2017abstracts/316_GC2017_High-Resolution_Biostratigraphic_and_XRF-Geochemical_Correlation.pdf

590 Li, Y. and Schieber, J. 2015. On the origin of a phosphate enriched interval in
591 the Chattanooga Shale Upper Devonian of Tennessee-A combined
592 sedimentologic, petrographic, and geochemical study. *Sedimentary*
593 *Geology*, *329*, 40–61.

594 Lynch, G. and Stasiuk, L. 2011. Characteristics of the Triassic Upper Montney
595 Tight Gas Play, Groundbirch Area , Northeast B.C. CSPG CSEG CWLS
596 Join Annual Convention: May 9-11 2011, Calgary, AB. Available from
597 http://www.cspg.org/cspg/documents/Conventions/Archives/Annual/2011/
598 169-Characteristics_of_Triassic_Upper_Montney_Tight_Gas.pdf

599 Marine Geoscience Data System (MGDS) website: http://www.marine-
600 geo.org/tools/GMRTMapTool/

601 Moslow, T.F. and Davies, G.R. 1997. Turbidite Reservoir Facies in the Lower
602 Triassic Montney Formation, West-Central Alberta. Bulletin of Canadian
603 Petroleum Geology, v. 45, p. 507–536.

604 Moslow, T.F., Haverslew, B., and Pelletier H., 2014. Lithofacies, Fabric
605 Selective Impacts on Reservoir Quality and Permeability Anisotropy in
606 Sedimentary Facies of the Montney Formation, Northeast British
607 Columbia. CSPG CSEG CWLS Joint Annual Convention, Calgary, 12-16
608 May 2014.

609 Moslow, T.F., Haverslew, B., and Henderson, C.M., 2016. Sedimentary facies,
610 petrology, conodont biostratigraphy and reservoir quality of a continuous

611 (395m) full diameter core of the Lower Triassic Montney Formation,
612 Northeastern British Columbia, Western Canada Sedimentary. In 2016
613 CSPG CSEG CWLS Convention - Core Conference Abstracts, p. 71–78.

614 Moslow, T. F., Haverslew, B. and Henderson, C. M. This volume. Sedimentary
615 facies, petrology, conodont biostratigraphy and reservoir quality of a
616 continuous 395 m full diameter core of the Montney Fm., Northeastern
617 BC. T. Euzen, T.F. Moslow and M. Caplan, (eds). The Montney Play:
618 Deposition to Development. CSPG Special Volume.

619 Nittrouer, C., Kuehl, S., Figueiredo, A.G., Allison, M., Sommerfield, C.K.,
620 Rine, J.M. and Silveira, O.M. 1996. The geological record preserved by
621 Amazon shelf sedimentation. Continental Shelf Research, 16(5–6), 817–
622 841. http://doi.org/10.1016/0278-4343(95)00053-4.

623 Orchard, M.J. and Tozer, E.T. 1997. Triassic conodont biochronology, its
624 calibration with the ammonoid standard, and a biostratigraphic summary
625 for the Western Canada Sedimentary Basin. Bulletin of Canadian
626 Petroleum Geology, v. 45, p. 675–692.

627 Orchard, M.J. and Zonneveld, J-P. 2009. The Lower Triassic Sulphur Mountain
628 Formation in the Wapiti Lake area: lithostratigraphy, conodont
629 biostratigraphy, and a new biozonation for the lower Olenekian (Smithian).
630 Canadian Journal of Earth Sciences, v. 46, p. 757–790.

631 Patruno, S., Hampson, G.J. and Jackson, C.A.L. 2015. Quantitative
632 characterisation of deltaic and subaqueous clinoforms. Earth-Science
633 Reviews, 142, 79–119.

634 Pauthier, S., Ducros, M., Chauveau, B. and Euzen, T. and Sassi, W. 2016.
635 Modeling source rock distribution, thermal maturation, petroleum retention
636 and expulsion: The Case of the Western Canadian Sedimentary Basin
637 (WCSB). AAPG Hedberg Conference, The Future of Basin and Petroleum
638 Systems Modeling, Santa Barbara, California, USA, April 3-6 2016.
639 Available from:
640 www.searchanddiscovery.com/abstracts/pdf/2016/90257hedberg/.../ndx_d
641 ucros.pdf

642 Rohais, S., Crombez, V., Euzen, T., Zonneveld, J.P. and Baudin, F. Subsidence
643 dynamic during the Montney Formation deposition (Lower Triassic,
644 Western Canada Sedimentary Basin): insights for its geodynamic setting
645 and wider implications. T. Euzen, T.F. Moslow and M. Caplan, (eds). The
646 Montney Play: Deposition to Development. CSPG Special Volume.

647 Sibuet, J.-C., Deffontaines, B., Hsu, S.-K., Thareau, N., Le Formal, J.-P., and
648 Liu, C.-S. 1998. Okinawa trough backarc basin: Early tectonic and
649 magmatic evolution. Journal of Geophysical Research: Solid Earth,
650 103(B12), 30245–30267. http://doi.org/10.1029/98JB01823

651 Tribovillard, N., Algeo, T.J., Lyons, T. and Riboulleau, A. 2006. Trace metals
652 as paleoredox and paleoproductivity proxies: an update. Chem. Geol. 232,
653 12-32. http:// dx.doi.org/10.1016/j.chemgeo.2006.02.012.

654 Wilson, N., Zonneveld, J.P. and Orchard M. 2012. Biostratigraphy of the
655 Montney Formation: From the Alberta and British Columbia Subsurface,
656 to the Outcrop. Geoconvention 2012: May 14-16 2012, Calgary, AB.
657 Available from
658 http://www.cspg.org/cspg/documents/Conventions/Archives/Annual/2012/
659 189_GC2012_Biostratigraphy_of_the_Montney_Formation.pdf

660 Wood, J. 2013. Water Distribution in the Montney Tight Gas Play of the
661 Western Canadian Sedimentary Basin: Significance for Resource
662 Evaluation. SPE Reservoir Evaluation & Engineering, 16(3), 290–302.
663 http://doi.org/10.2118/161824-PA

664 Zonneveld, J., Golding, M., Moslow, T.F., Orchard, M.J., Playter, T. and
665 Wilson, N. 2011. Depositional Framework of the Lower Triassic Montey
666 Formation , West-central Alberta and Northeastern British Columbia (oral
667 presentation). CSPG CSEG CWLS Join Annual Convention: May 9-11
668 2011, Calgary, AB. Available from:
669 http://www.cspg.org/cspg/documents/Conventions/Archives/Annual/2011/
670 323-Depositional_Framework_of_Lower_Triassic_Montey_Fm.pdf

671 Zonneveld, J.P., and Moslow, T.F. 2014. Perennial River Deltas of the Montney
672 Formation: Alberta and British Columbia Subcrop Edge. In 2014 CSPG
673 CSEG CWLS Convention - Core Conference Abstracts p. 25–26.

674 Zonneveld, J.P., Furlong, C.M., Gegolick, A., Gingras, M., Golding, M.,
675 Moslow, T.F., Orchard, M., Playter, T., Prenoslo, D. and Sanders, S.C.
676 2016. The Montney-Doig Boundary and the "Anisian wedge". In 2016
677 CSPG CSEG CWLS Convention - Core Conference Abstracts, p. 63–66.

678

679

FIGURE CAPTIONS

Figure 1: Stratigraphic Chart of the Montney Formation (Embry and Gibson, 1995; Davies et al., 1997; Golding et al., 2014; Crombez et al., 2016a and 2016b; Davies and Hume, 2016; Moslow et al., 2016, Henderson and Schoepfer, 2017). A.W.: 'Anisian Wedge'; D.P.: Doig 'Phosphatic Member'; Wavy red line: angular unconformity.

Figure 2: Location map of the database wells used in this study and selected cores illustrated in figures 3, 4, 6, 7 and 9. Oil and gas fields cited in this paper are also shown.

Figure 3: Core and log expression of Spathian flooding surfaces from well a-94-J/94-A-13. Note the consistency between the total Gamma Ray curve and the Uranium concentration measured from core. See Fig. 7 for legend of lithology and depositional environments.

Figure 4: Core and log expression of Spathian flooding surfaces from well d-97-C/94-G-7. Note that most of the low API value Gamma Ray log spikes correspond to dolosiltstone intervals. See Fig. 7 for legend of lithology and depositional beds.

Figure 5: Internal stratigraphic architecture of the Spathian deposits along six depositional dip-oriented regional cross-sections. Logs are Gamma Ray curves and vertical bars indicate cored intervals.

Figure 6: Representative core photos of depositional facies. A - Lower shoreface: sharp based, normally graded, planar laminated, silty very-fine grained sandstone bed in middle of photograph (brackets) is inferred to be the product of upper flow

regime transport and a waning of flow by a storm generated current, thus interpreted to be a tempestite. Note Bergaueria burrow traces at top of the bed (arrows). Tempestite bed is overlain and underlain by densely burrowed to bioturbated coarse -grained siltstones. Core diameter is 10cm. B - Offshore Transition: planar -to low relief ripple - laminated coarse-grained siltstone. Note lateral discontinuity in planar laminations (ellipse) possibly due to crypto-bioturbation; also note minor degree of load-casting at base of lenticular bed (arrow). Core diameter is 7.5cm. C – Offshore: Massive - appearing to faintly parallel laminated highly bituminous to kerogenous fine-to medium- grained siltstone. Sedimentation is a product of suspension deposition seaward of mean storm-weather wave base. Core diameter is 7.5cm. D – Hemipelagite: laminated calcite-cemented bioclastic dolosiltstone; bioclasts occur as 0.5-1.0mm calcispheres (dinoflagellates?); note inverse grading from base of bed (arrow) and increase in the carbonate/clastic ratio upwards. Core diameter is 7.5cm.

Figure 7: Core descriptions and interpretation of the main sedimentary facies associations observed in the Spathian deposits displaying the lateral facies heterogeneity observed within individual parasequence sets (see Fig. 2 for the location of wells). a) Topset setting (proximal offshore transition to lower shoreface); b) Foreset setting (distal offshore transition to offshore); c) Bottomset setting (Offshore).

Figure 8: Diagram illustrating the depositional environments and paleobathymetric relief of clinoforms in the lower part of the Spathian.

Figure 9: Vertical stacking pattern of facies and depositional environments based on sedimentologic description of full diameter core (Moslow et al., this volume) and calibration to gamma ray log signature of the Spathian interval from three wells in the study area. Wells are arranged in proximal to distal setting from right to left. Purple arrows on the right side of each well highlight the occurrence of hemipelagite dolosiltstone beds. Pie charts quantify the vertical and lateral gradation of facies and depositional environments for individual parasequence sets. Note volumetric increase in shallow water facies upwards inferring a progradational trend in the Spathian.

Figure 10: Regional isopach maps of parasequence sets M3-1 to M3-4. The maps only highlight the areas where thickness exceeds 10 m, which corresponds roughly to the foreset area of each unit.

Figure 11: Regional strike-oriented 330 km-long cross-section of the Montney Formation, with Spathian internal units. Wireline logs are are Gamma Ray curves. Insert map shows major structural elements from Berger et al. (2008).

Figure 12: Paleogeographic reconstruction of the depositional environment during lower Spathian times.

Figure 13: Five regional dip-oriented cross-sections in west-central Alberta and northeastern British Columbia illustrating the internal stratigraphic architecture of the Montney Formation and Spathian internal units at regional scale.

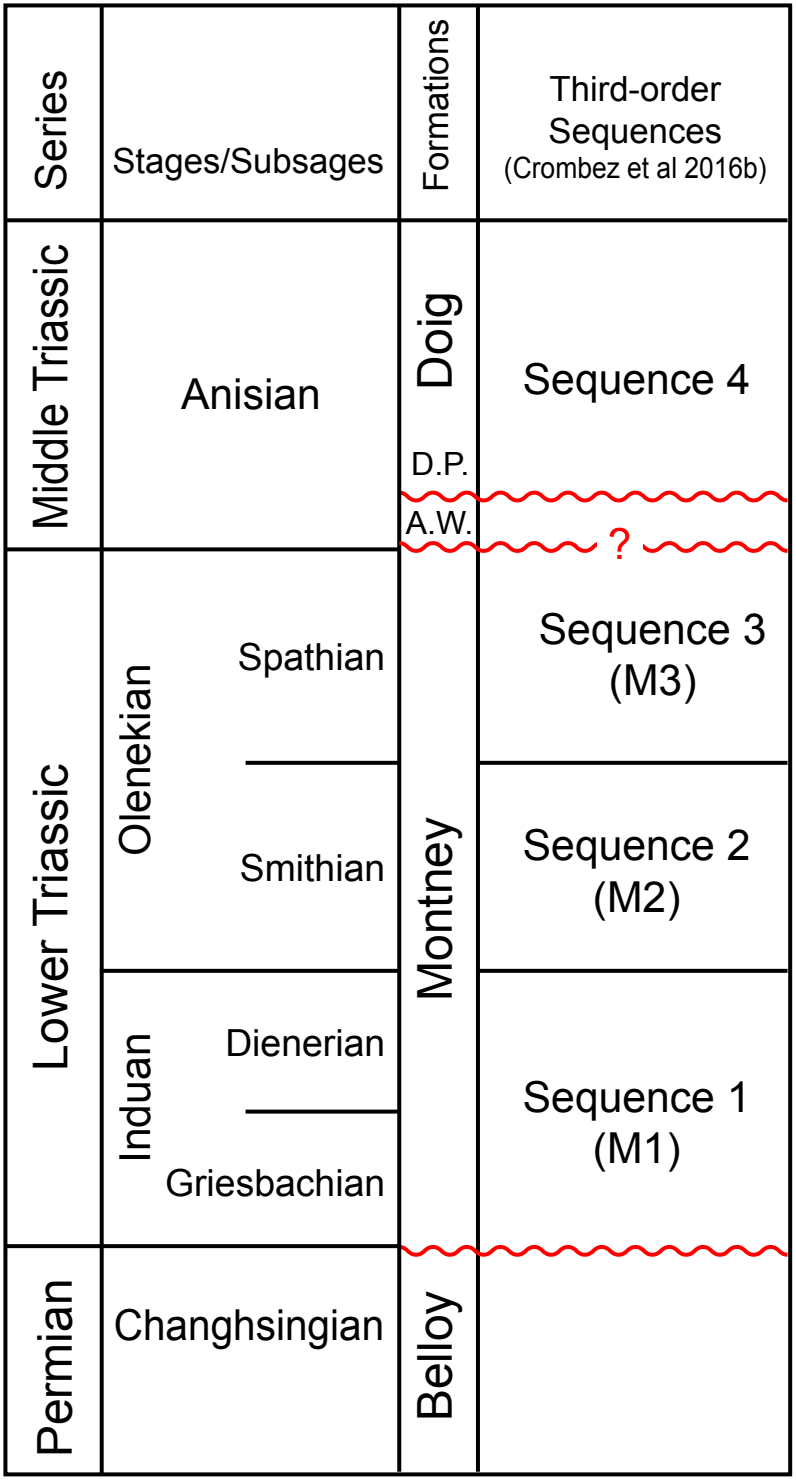
Series
Stages/Subsages
Formations
Third-order Sequences (Crombez et al 2016b)
Middle Triassic
Anisian
Doig
Sequence 4
D.P.
A.W.
?
Lower Triassic
Olenekian
Spathian
Smithian
Sequence 3 (M3)
Sequence 2 (M2)
Montney
Induan
Dienerian
Griesbachian
Sequence 1 (M1)
Permian
Changhsingian
Belloy

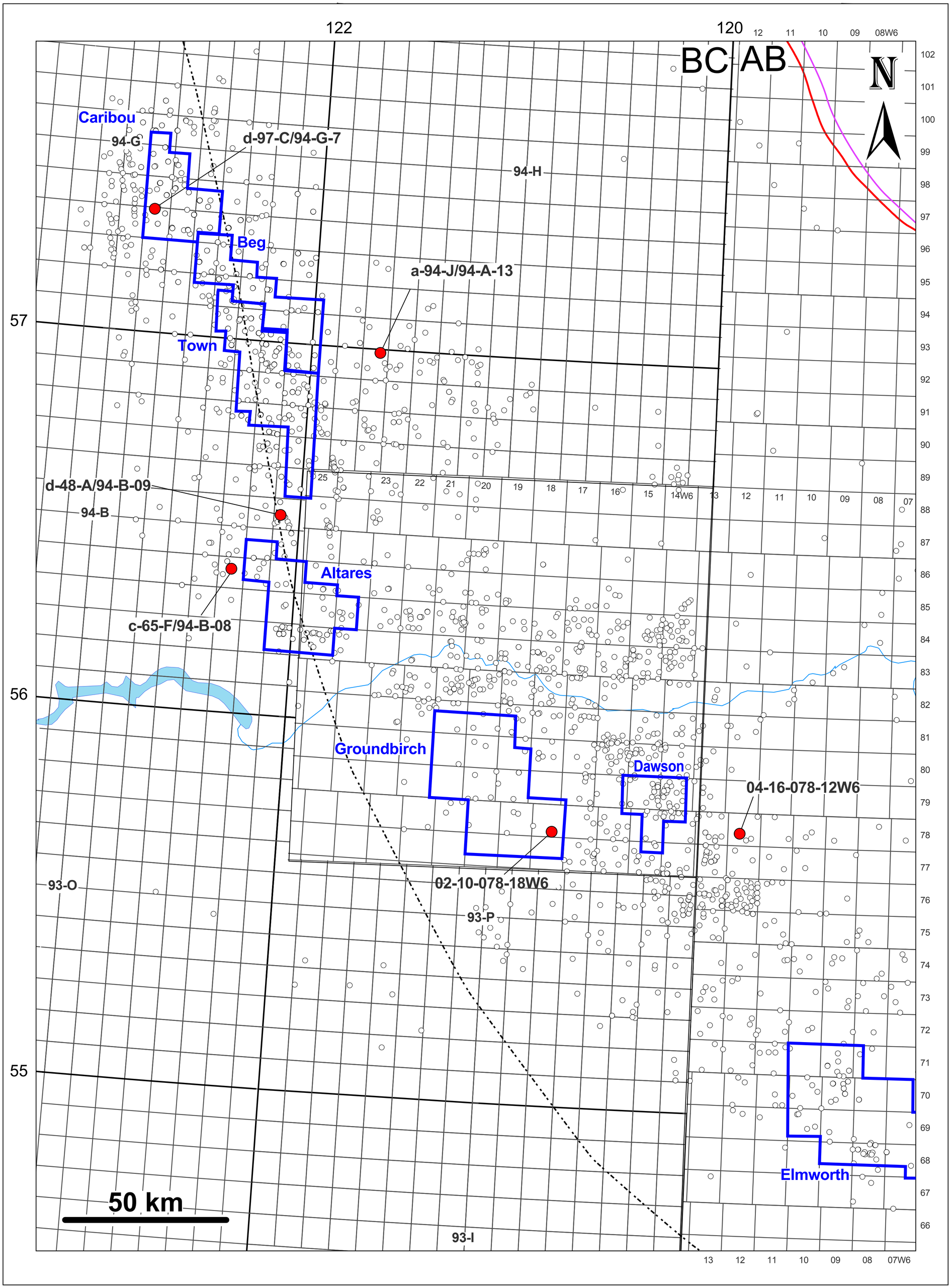

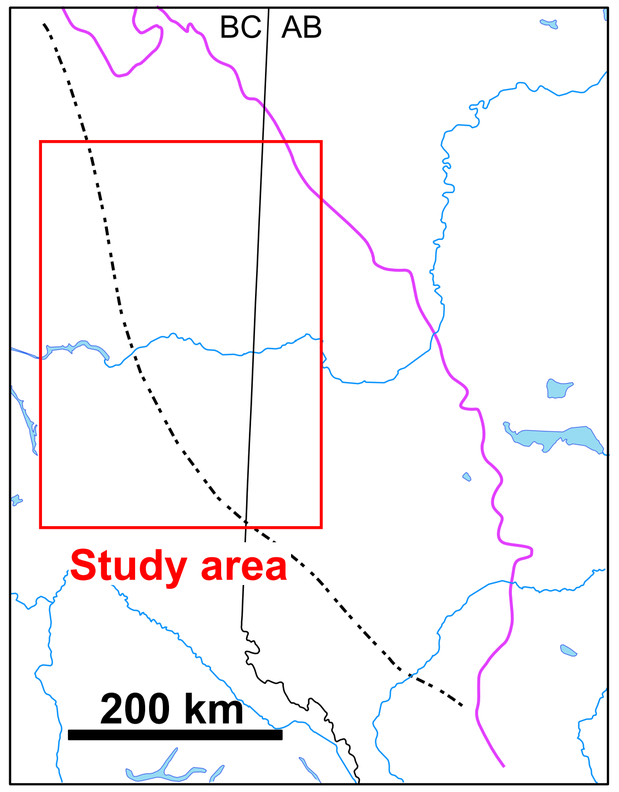

Montney subcrop edge

Cordillera deformation front

Well data

Core data

Fields cited in this study

Core Gamma Ray (UG)

Wireline Gamma Ray (API)

Core description

U-Core (ppm)

K-Core (%)

Th-Core (ppm)

Depth (m)

Flooding Surface (M3-2)

Flooding Surface (M3-1)

Cruziana trace fossil assemblage; diminutive, low diversity forms

TOC 1-2%

Skolithos (distal) assemblage, proximal tempestites

Dolosiltstone

Phosphatic lag

Interbedded F-M / M-C sandy siltstone; highly bituminous; TOC 5.5%; SSD at contact; non burrowed; seismites

TOC 4.4%

Distal Cruziana with a decrease in abundance and diversity of traces; phosphate clasts

Distal tempestites; distal Cruziana

Bituminous F-C siltstone; TOC 4.3%

Distal Cruziana trace fossil assemblage; distal tempestites; diminutive traces

Bituminous siltstone (TOC=4.3%)

1647.30

1652.10

M3-1

50 cm

Distal tempestites

Proximal tempestites

Dolosiltstone

Phosphatic lag (M3-2)

1637.70

1640.10

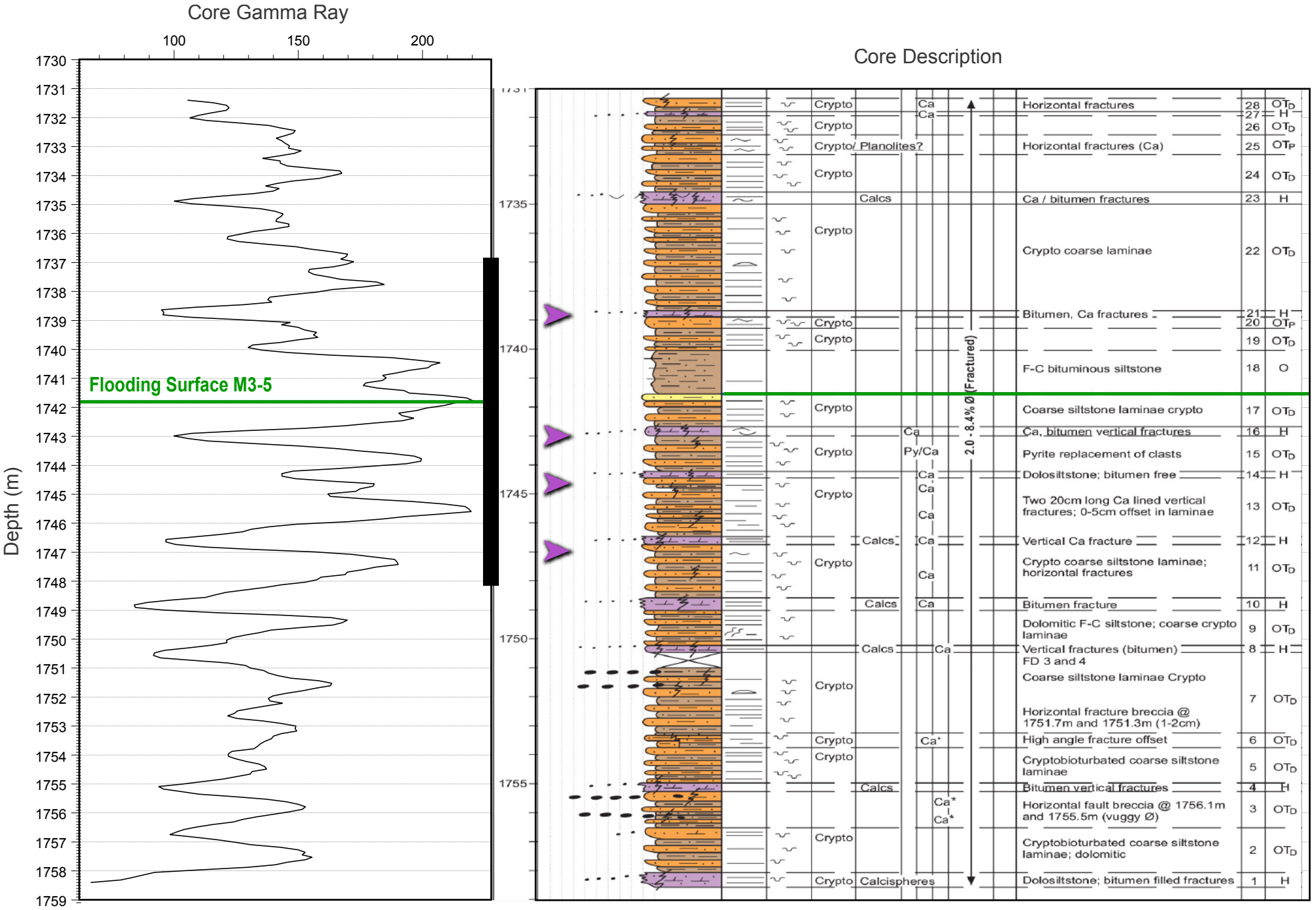

1736.73

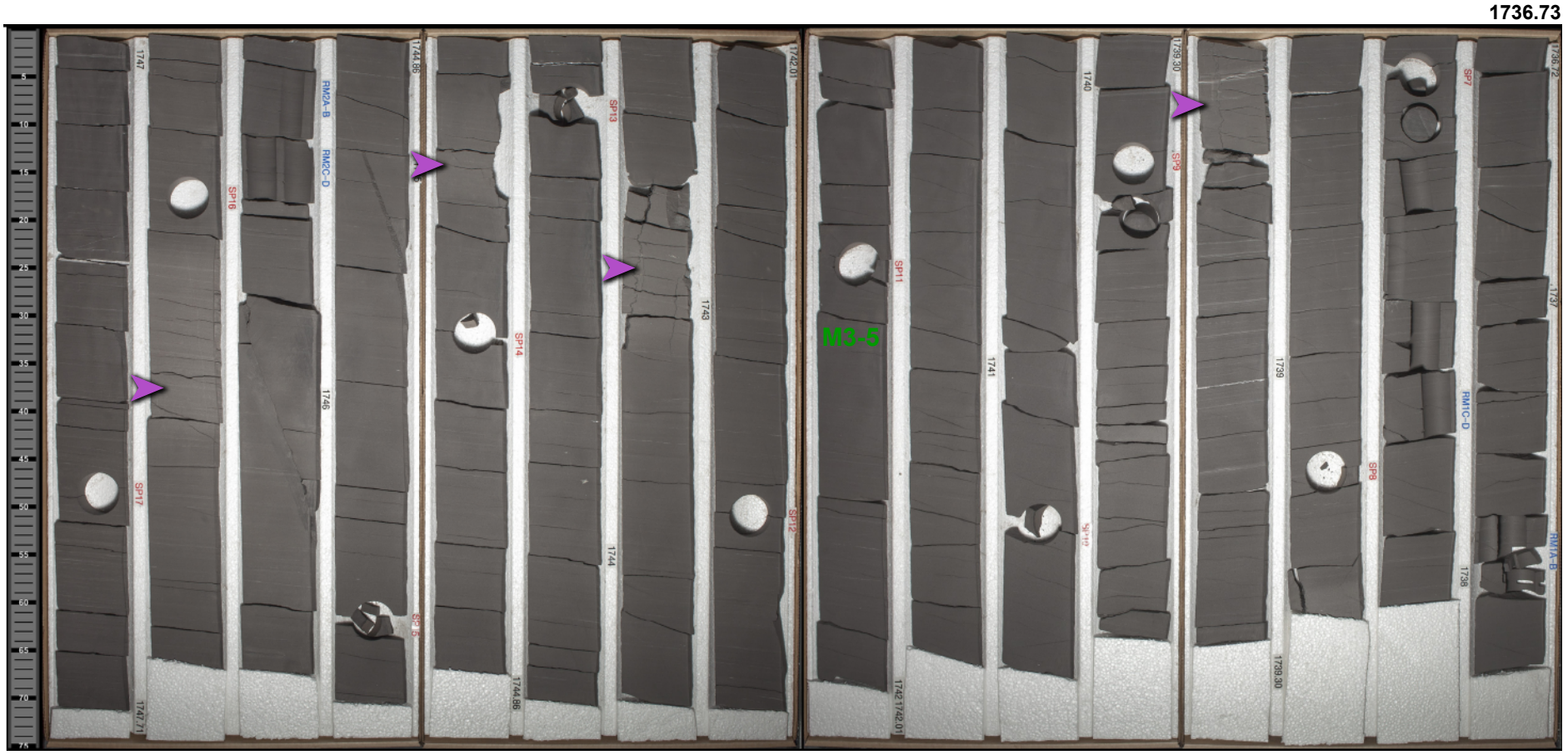

1747.71

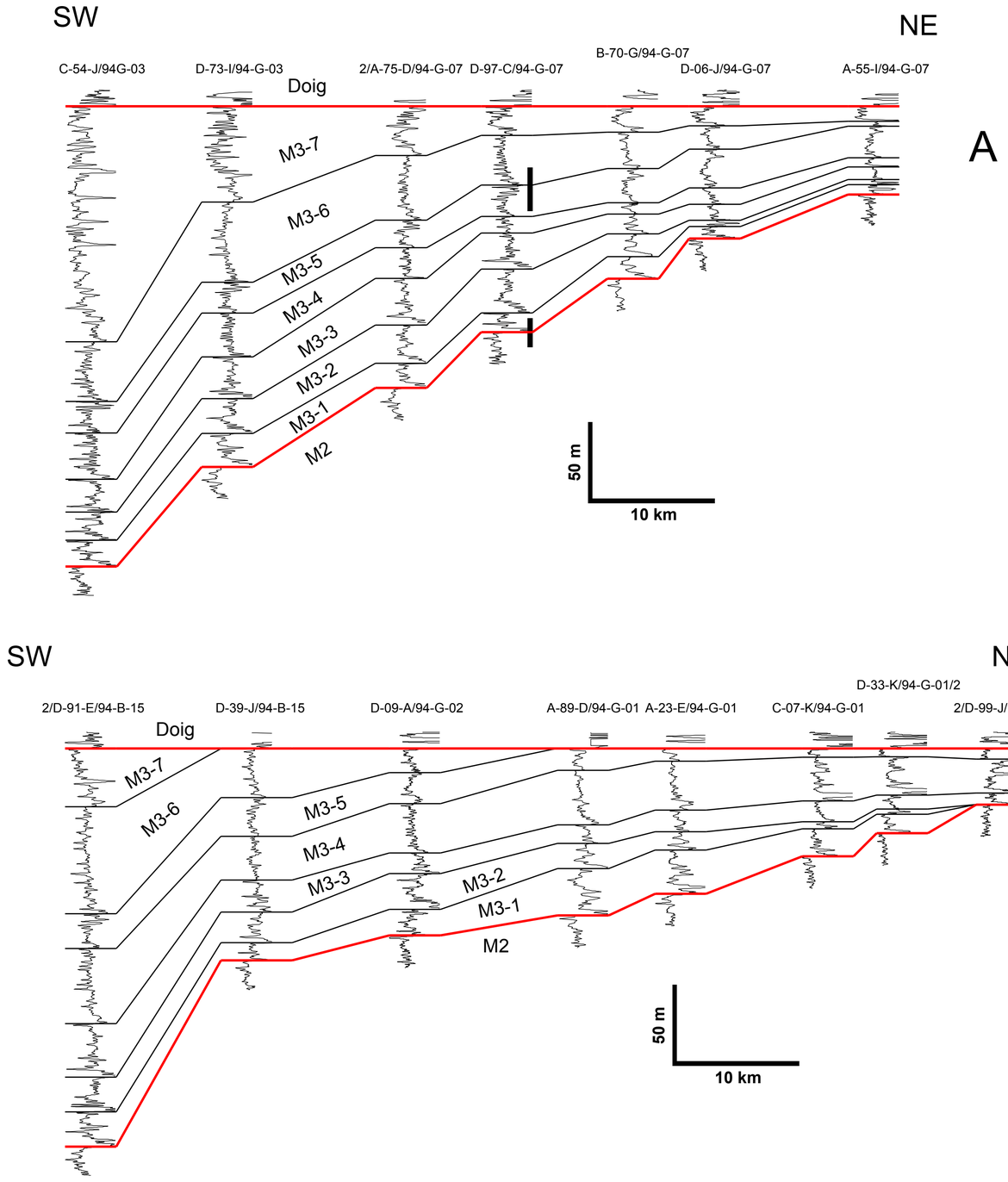
SW
NE
C-54-J/94G-03
D-73-I/94-G-03
2/A-75-D/94-G-07
D-97-C/94-G-07
B-70-G/94-G-07
D-06-J/94-G-07
A-55-I/94-G-07
Doig
M3-7
M3-6
M3-5
M3-4
M3-3
M3-2
M3-1
M2
50 m
10 km
A
SW
NE
2/D-91-E/94-B-15
D-39-J/94-B-15
D-09-A/94-G-02
A-89-D/94-G-01
A-23-E/94-G-01
D-33-K/94-G-01/2
C-07-K/94-G-01
2/D-99-J/94-G-01
Doig
M3-7
M3-6
M3-5
M3-4
M3-3
M3-2
M3-1
M2
50 m
10 km
B

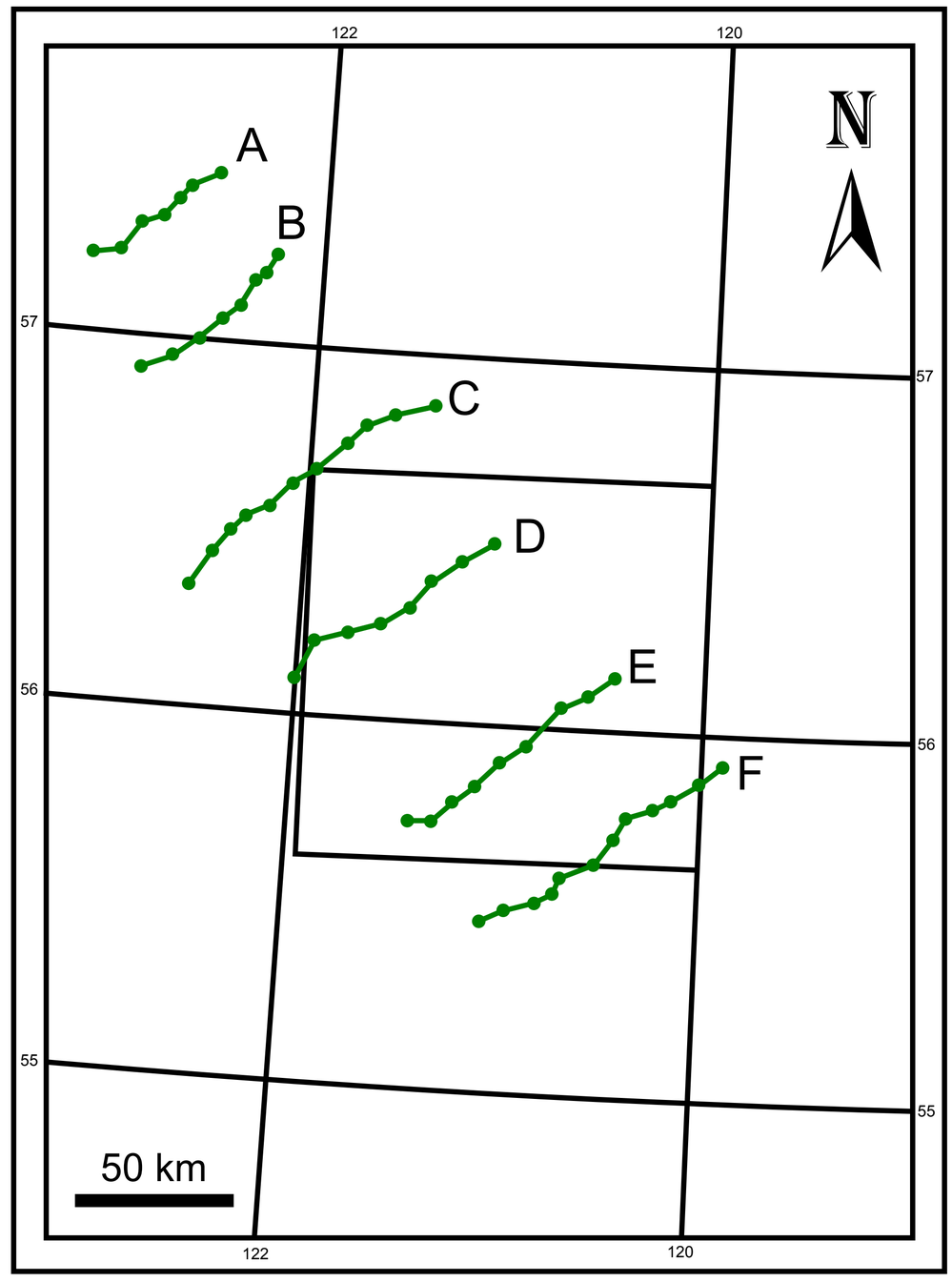
122
120
57
56
55
N
A
B
C
D
E
F
50 km

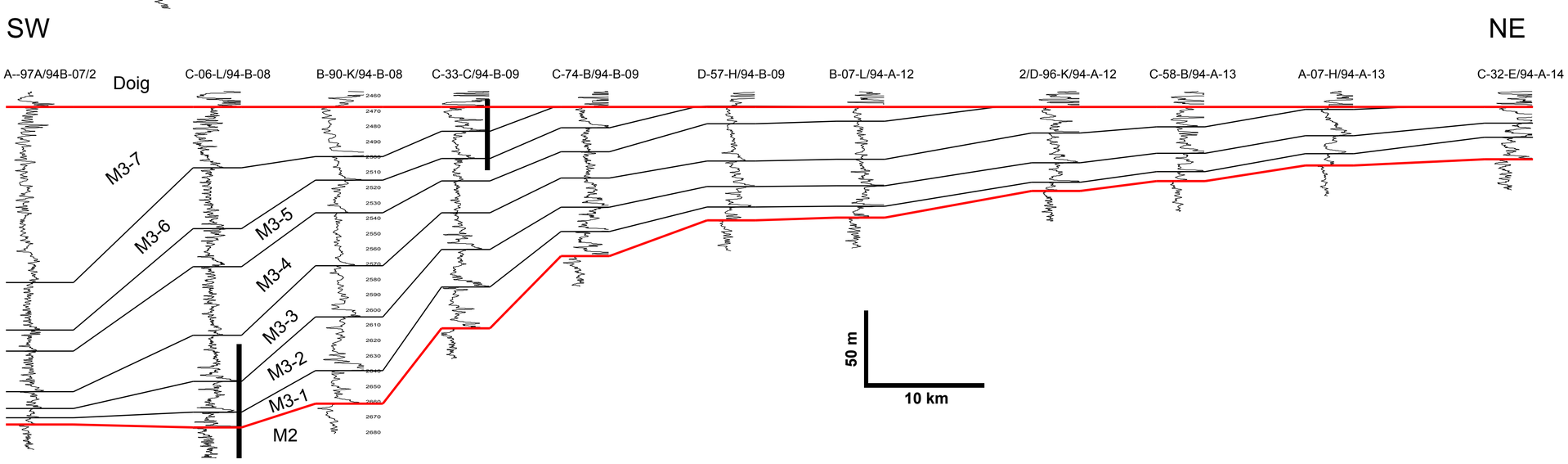
SW
NE
A--97A/94B-07/2
C-06-L/94-B-08
B-90-K/94-B-08
C-33-C/94-B-09
C-74-B/94-B-09
D-57-H/94-B-09
B-07-L/94-A-12
2/D-96-K/94-A-12
C-58-B/94-A-13
A-07-H/94-A-13
C-32-E/94-A-14
Doig
M3-7
M3-6
M3-5
M3-4
M3-3
M3-2
M3-1
M2
50 m
10 km
C

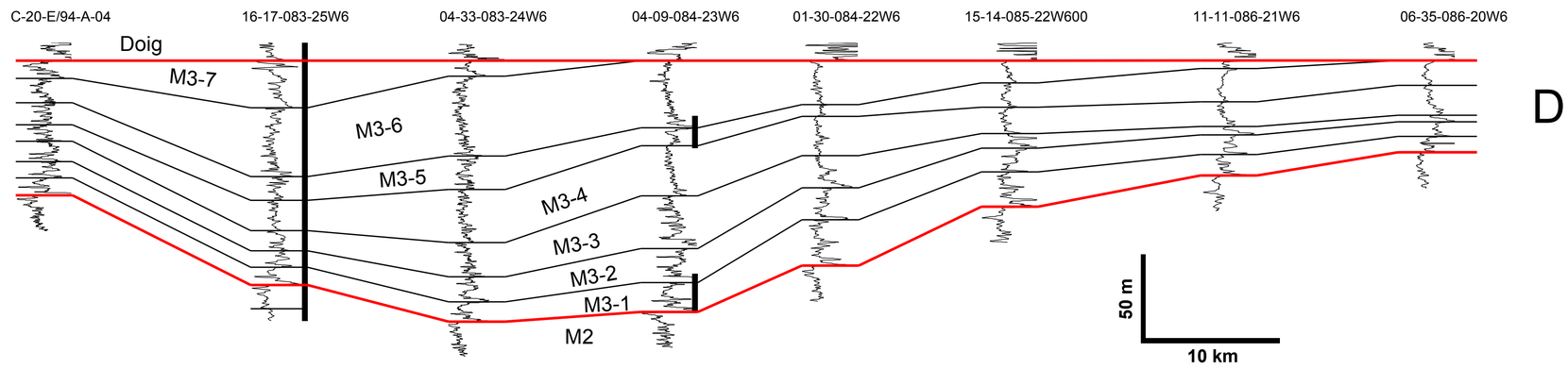
SW
NE
C-20-E/94-A-04
16-17-083-25W6
04-33-083-24W6
04-09-084-23W6
01-30-084-22W6
15-14-085-22W600
11-11-086-21W6
06-35-086-20W6
Doig
M3-7
M3-6
M3-5
M3-4
M3-3
M3-2
M3-1
M2
50 m
10 km
D

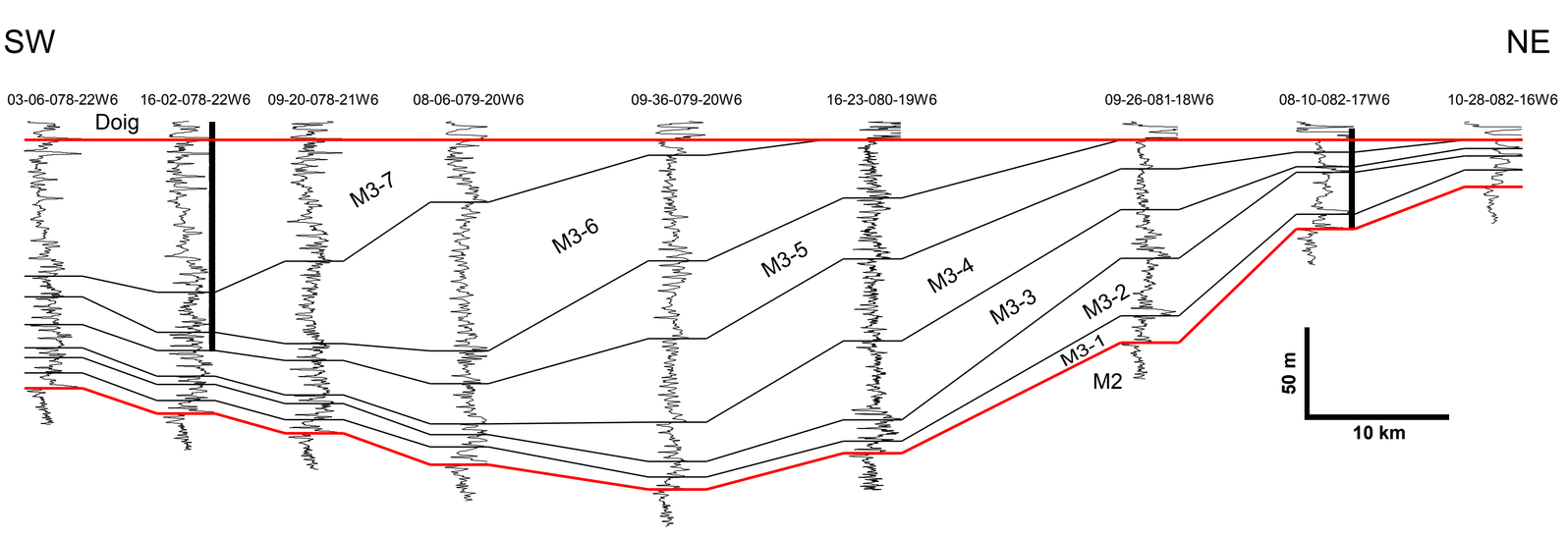
SW
NE
03-06-078-22W6
16-02-078-22W6
09-20-078-21W6
08-06-079-20W6
09-36-079-20W6
16-23-080-19W6
09-26-081-18W6
08-10-082-17W6
10-28-082-16W6
Doig
M3-7
M3-6
M3-5
M3-4
M3-3
M3-2
M3-1
M2
50 m
10 km
E

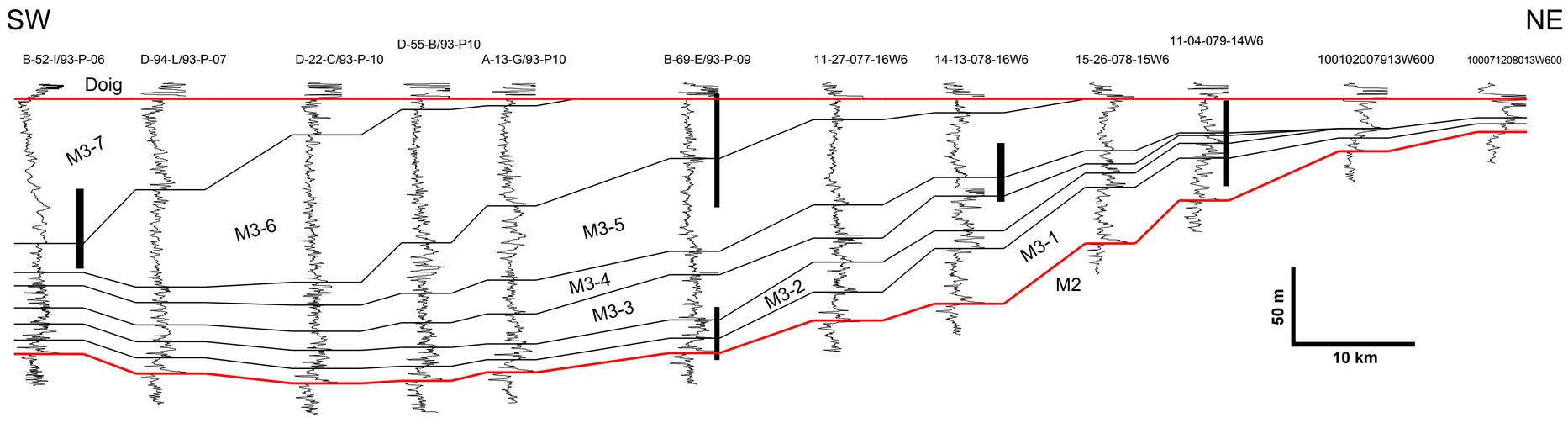
SW
NE
B-52-I/93-P-06
D-94-L/93-P-07
D-22-C/93-P-10
D-55-B/93-P10
A-13-G/93-P10
B-69-E/93-P-09
11-27-077-16W6
14-13-078-16W6
11-04-079-14W6
15-26-078-15W6
100102007913W600
100071208013W600
Doig
M3-7
M3-6
M3-5
M3-4
M3-3
M3-2
M3-1
M2
50 m
10 km
F

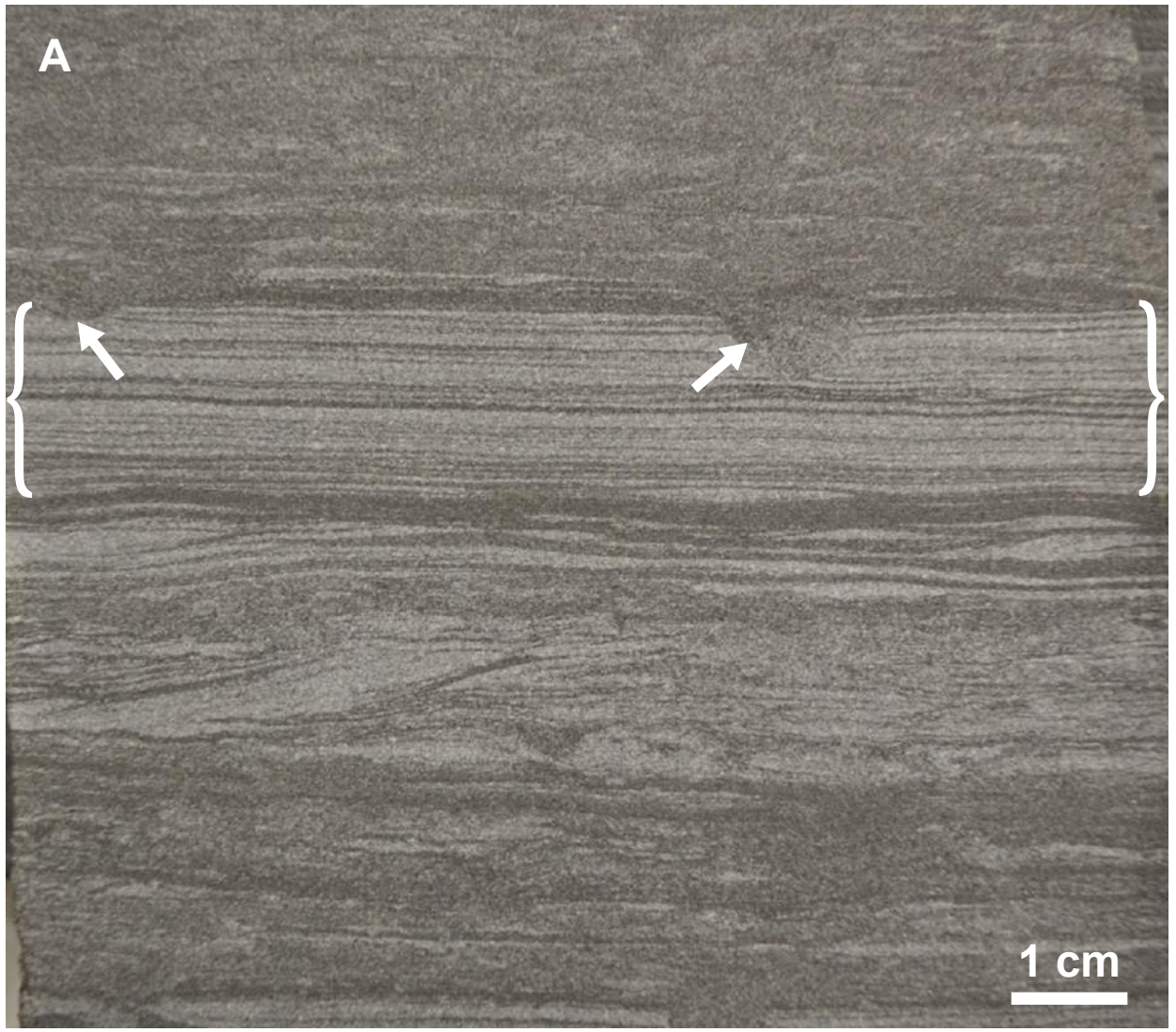
A
1 cm

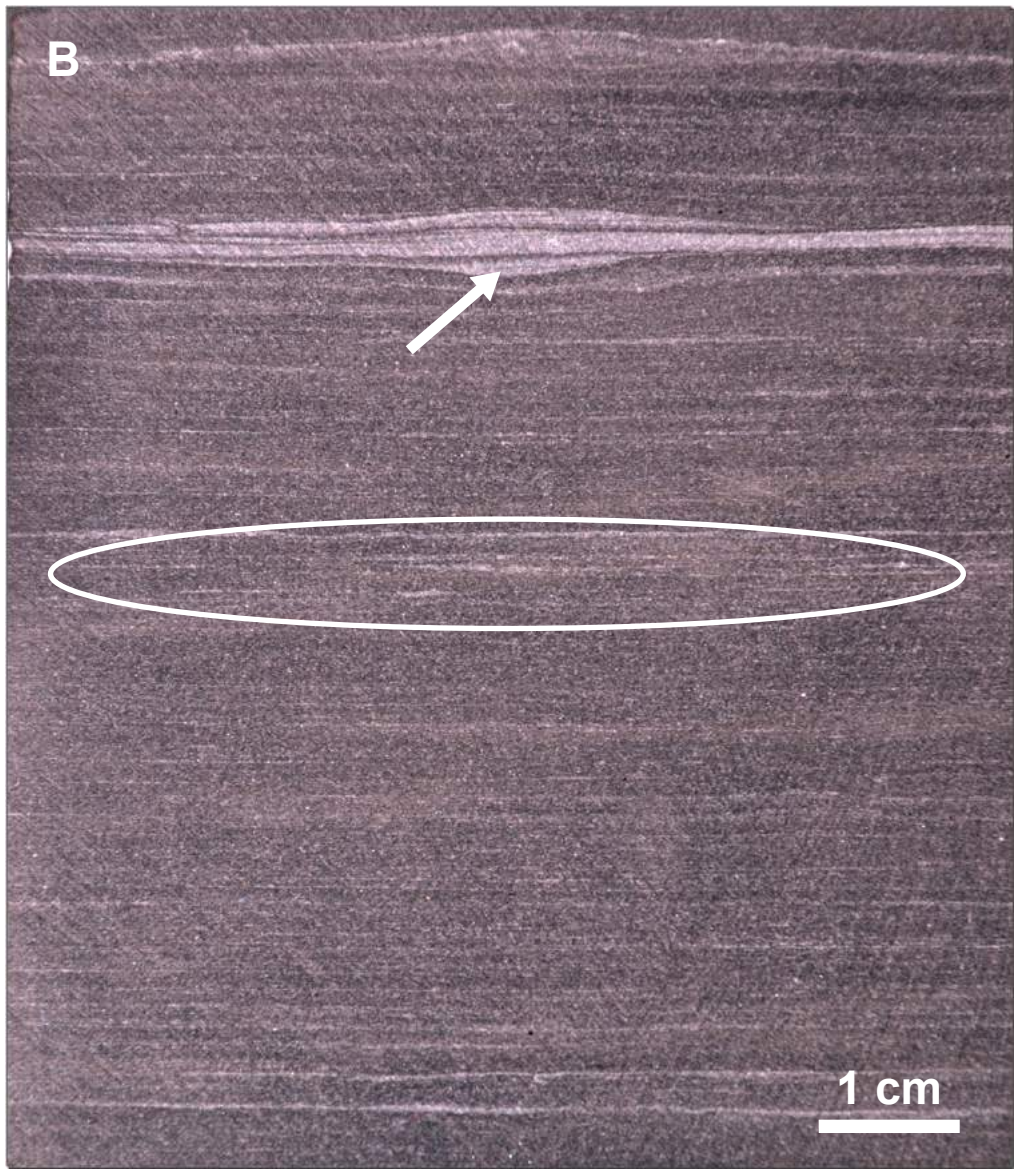
B
1 cm

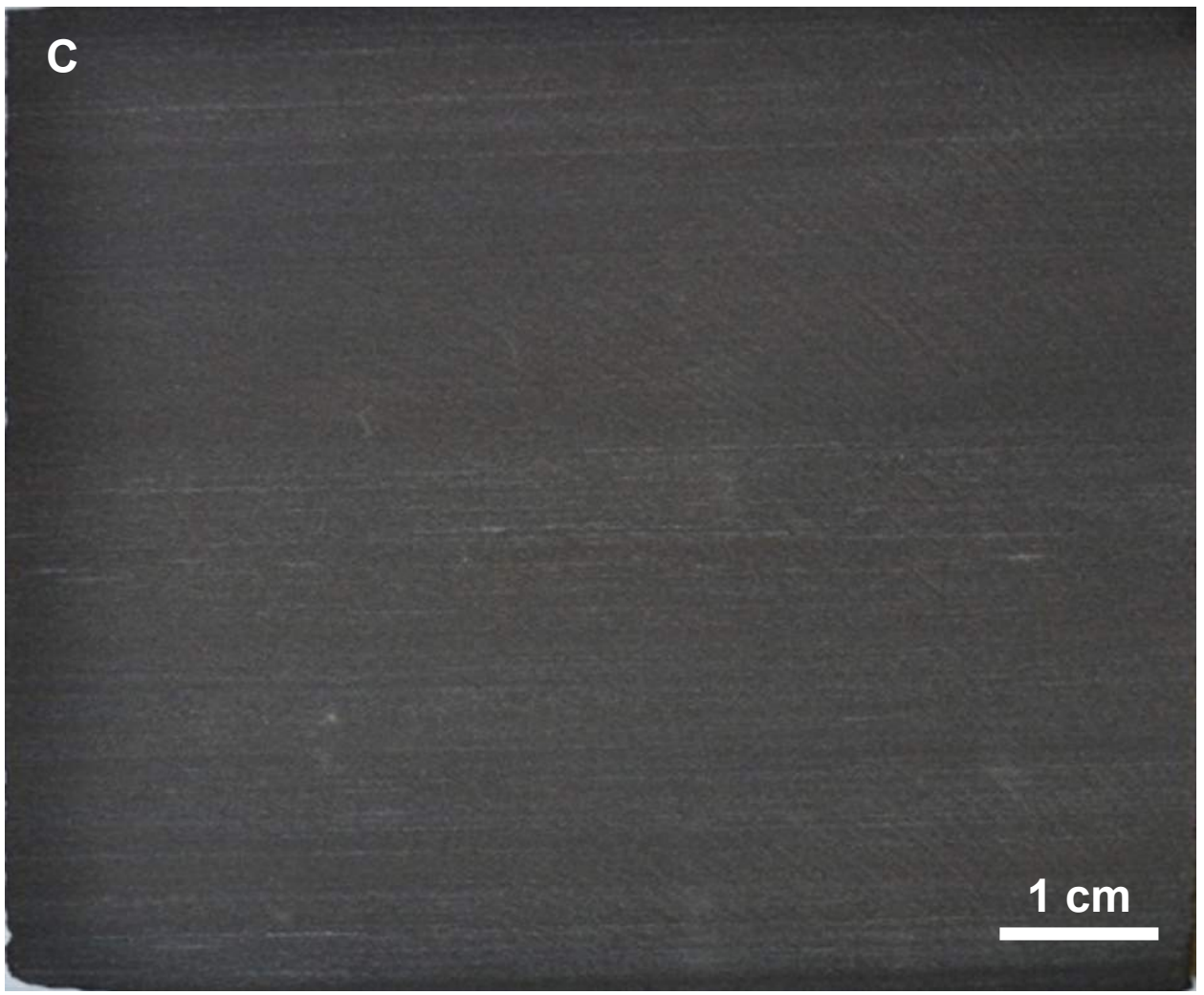
C
1 cm

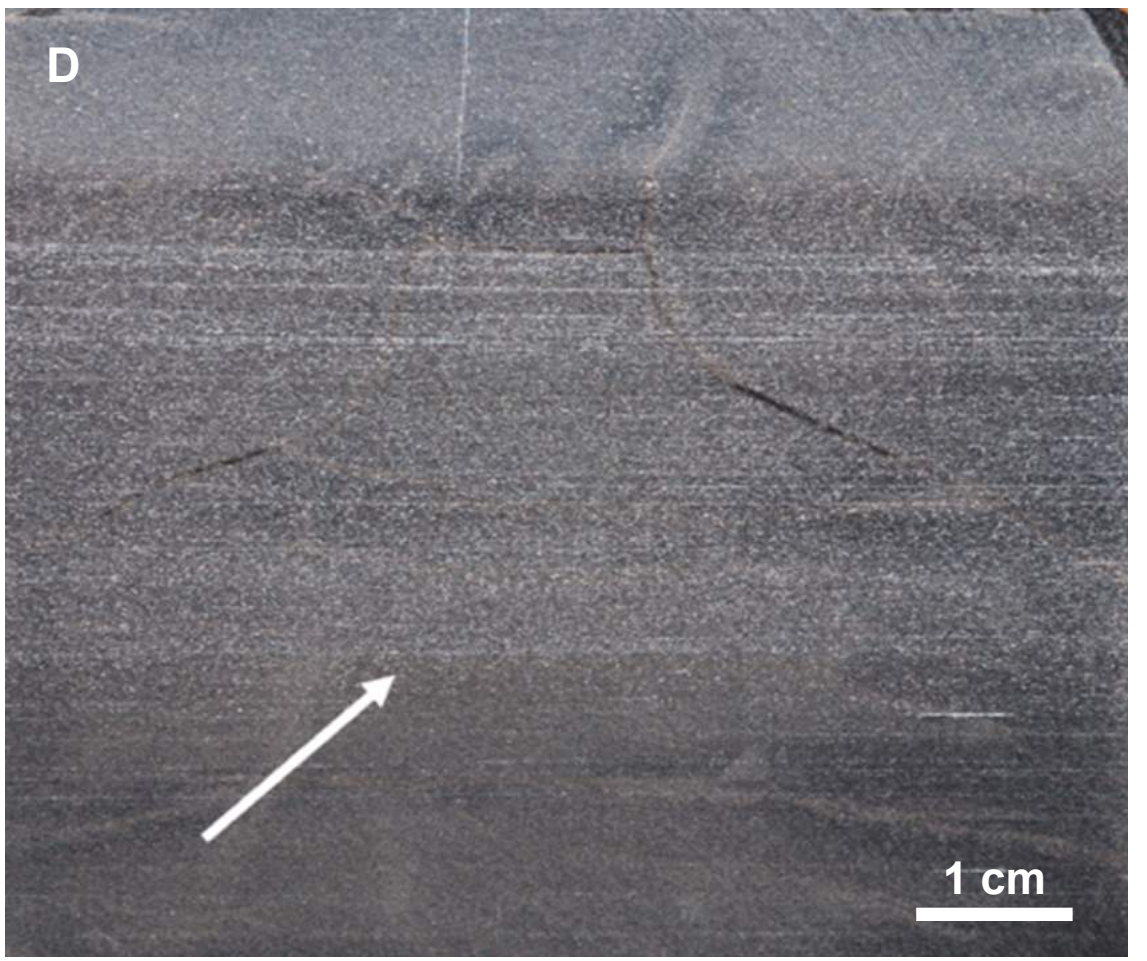
D
1 cm

ⓒ

02-10-078-18W6

Bottomset setting facies association

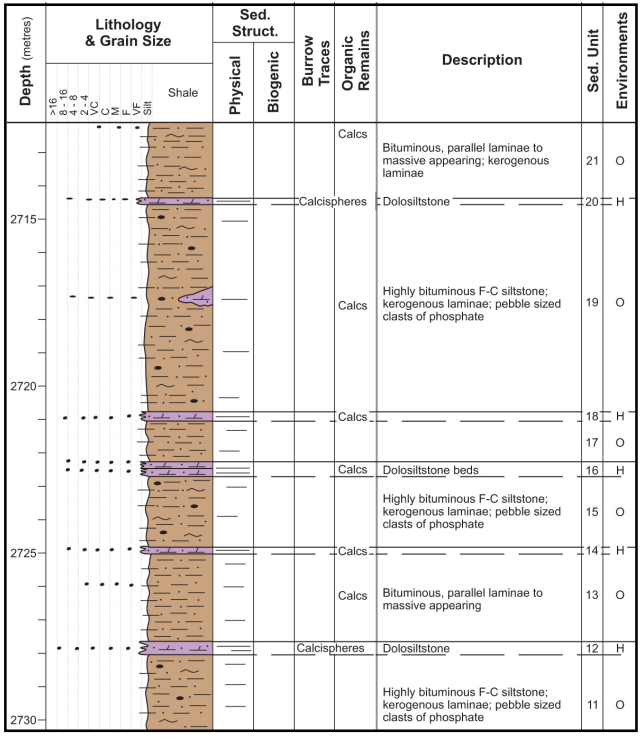

ⓑ

c-65-F/94-B-08

Foreset setting facies association

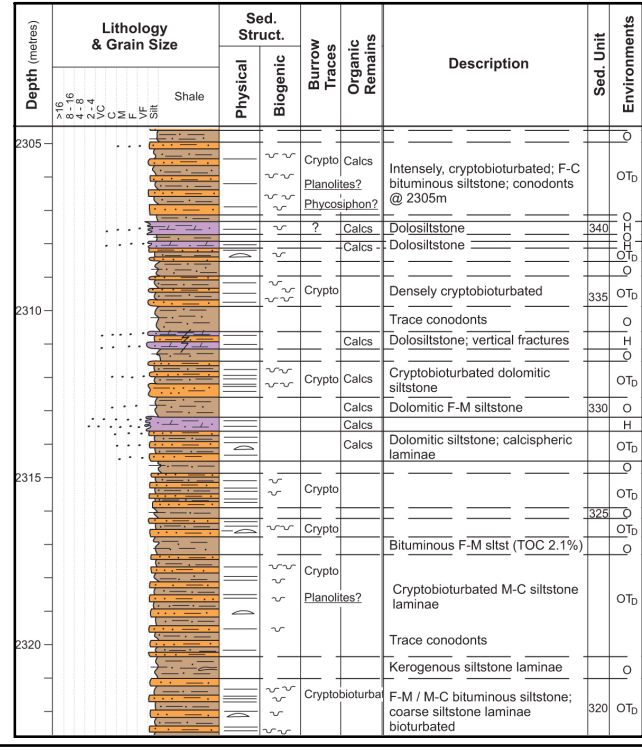

ⓐ

a-94-J/94-A-13

Topset setting facies association

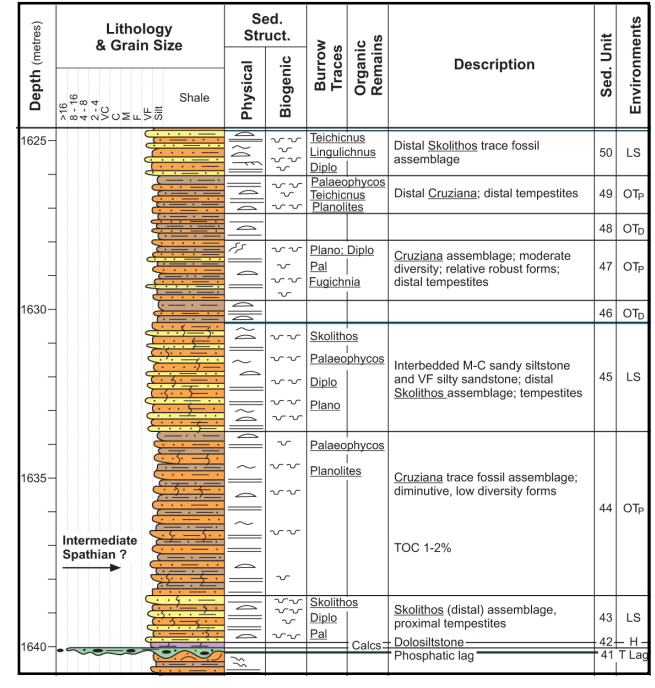

Sedimentary Facies

Bituminous F-M Siltstone
(massive appearing to faintly parallel laminated)

Calcareous, Calcispheric Dolosiltstone

Sandy F-C Siltstone
(rippled, planar laminated, wavy bedded; macro-scale burrowing)

F-C Siltstone
(planar laminated, lenticular bedded, burrowed to cryptobioturbated)

Environments of Deposition

LS: Lower Shoreface

OT_P: Proximal Offshore Transition

OT_D: Distal Offshore Transition

O: Offshore

H: Hemipelagite

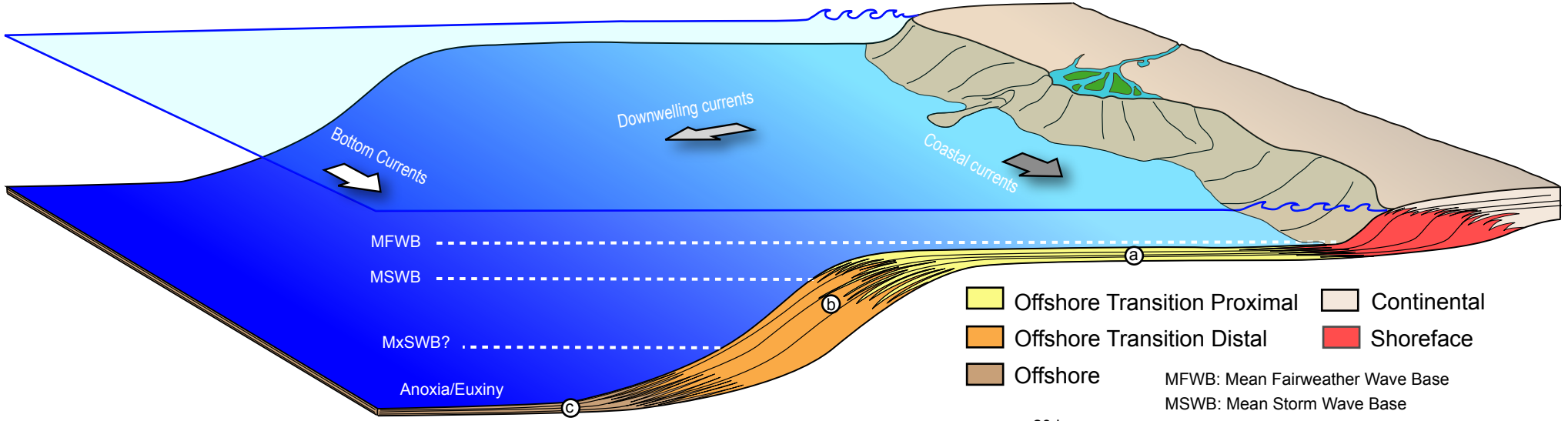
Bottom Currents
Downwelling currents
Coastal currents
MFWB
MSWB
MxSWB?
Anoxia/Euxiny
a
b
c
Offshore Transition Proximal
Offshore Transition Distal
Offshore
Continental
Shoreface
20 km
MFWB: Mean Fairweather Wave Base
MSWB: Mean Storm Wave Base
MxSWB: Maximum Storm Wave Base
ⓐ Core descriptions (Fig. 7)

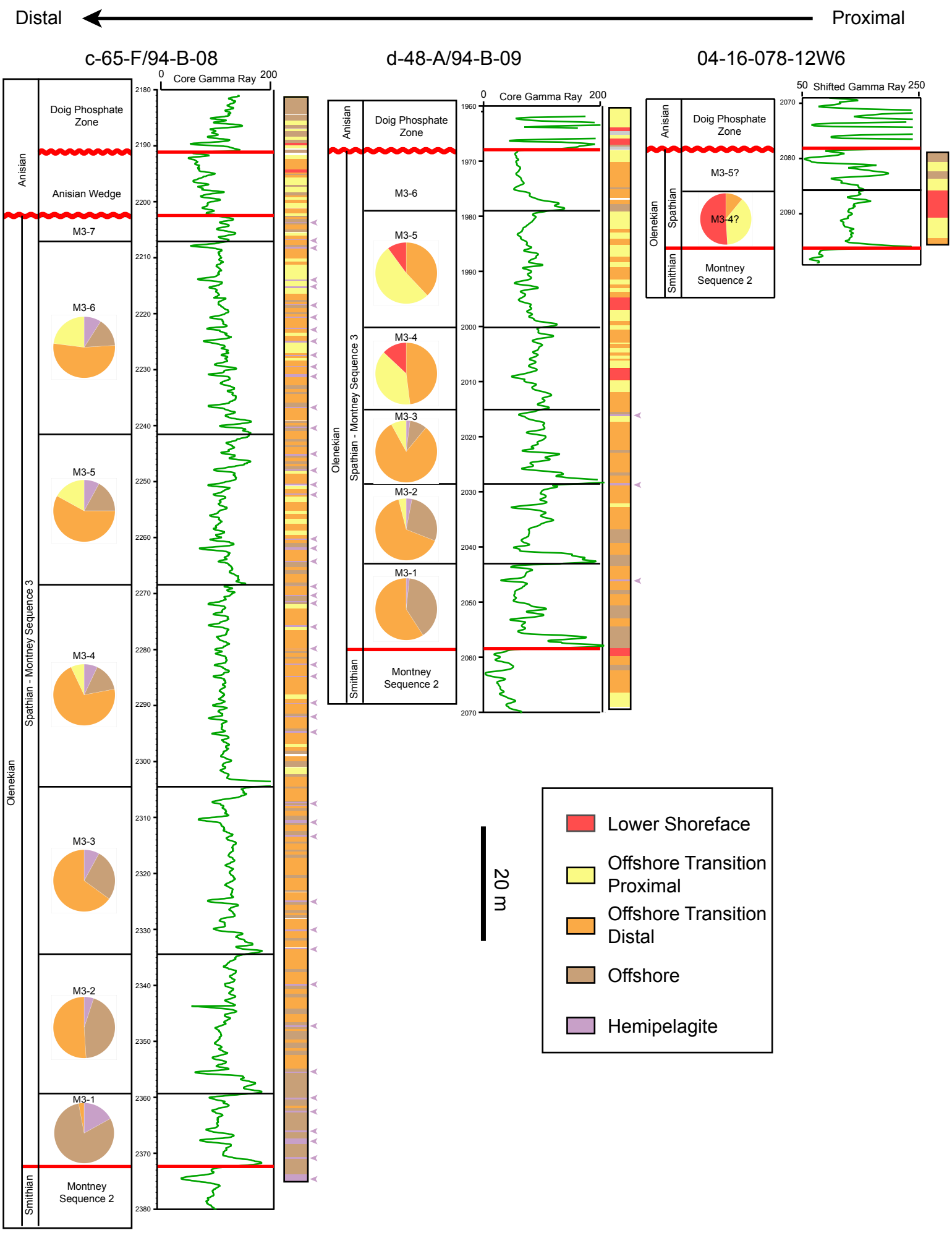
Distal
Proximal
c-65-F/94-B-08
d-48-A/94-B-09
04-16-078-12W6
Core Gamma Ray
Shifted Gamma Ray
Anisian
Olenekian
Spathian - Montney Sequence 3
Smithian
Doig Phosphate Zone
Anisian Wedge
M3-7
M3-6
M3-5
M3-4
M3-3
M3-2
M3-1
M3-5?
M3-4?
Montney Sequence 2
20 m
Lower Shoreface
Offshore Transition Proximal
Offshore Transition Distal
Offshore
Hemipelagite

M3-1

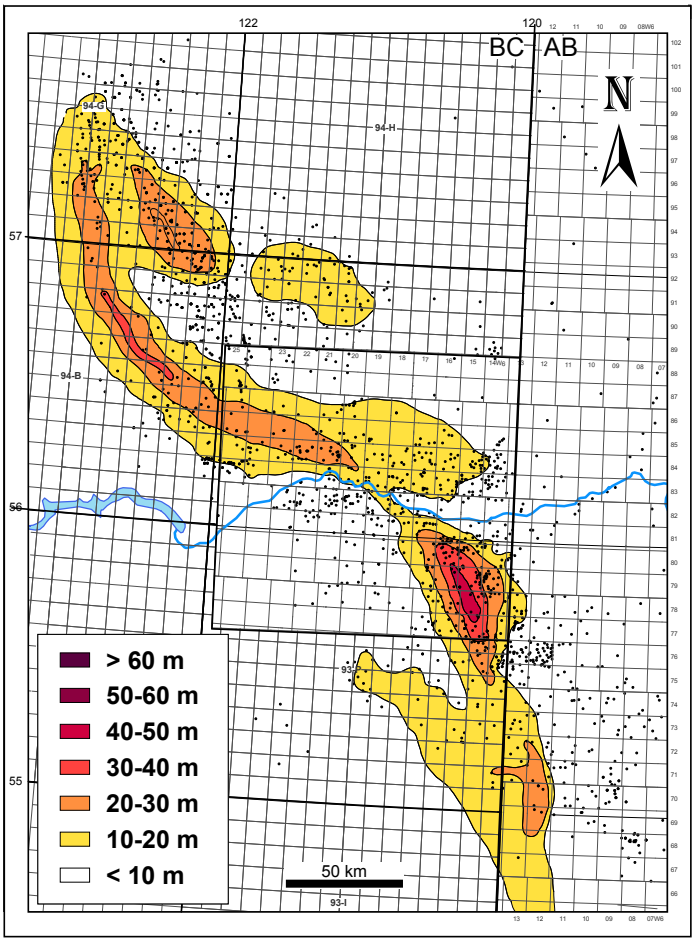

M3-2

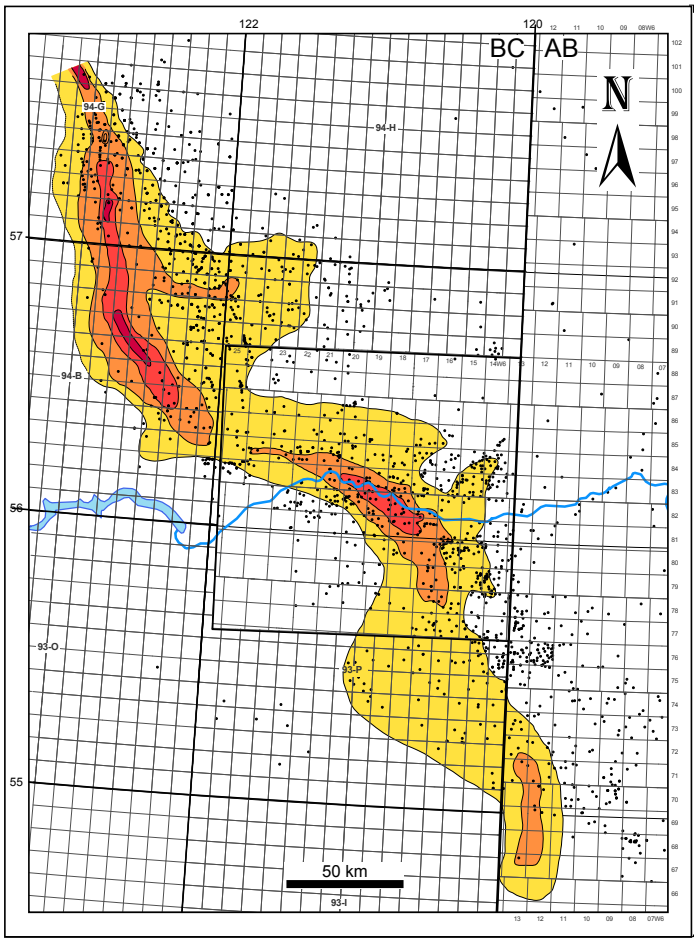

M3-3

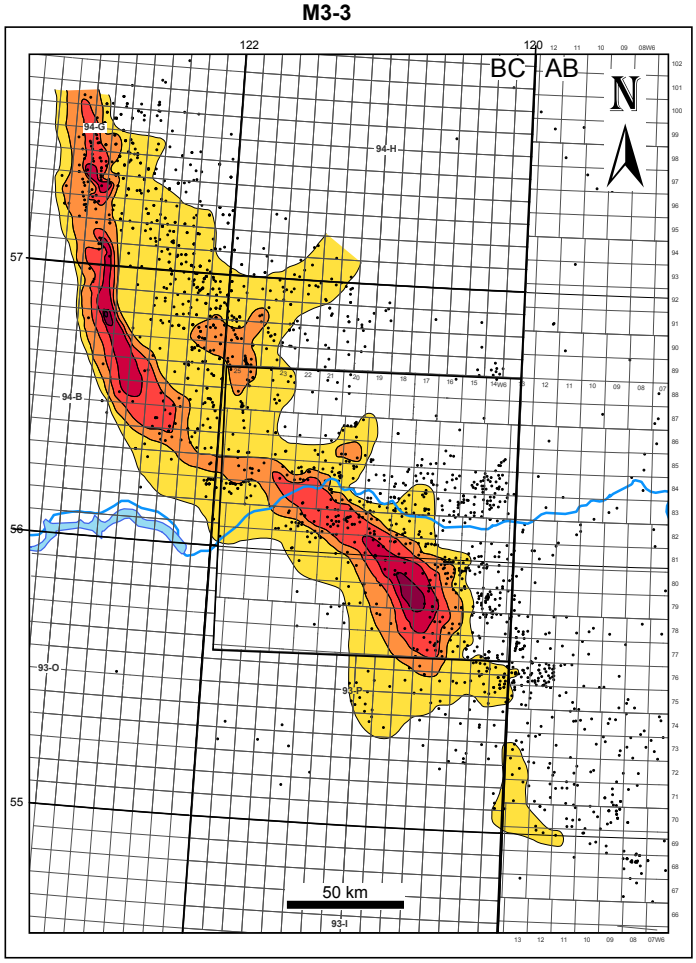

M3-4

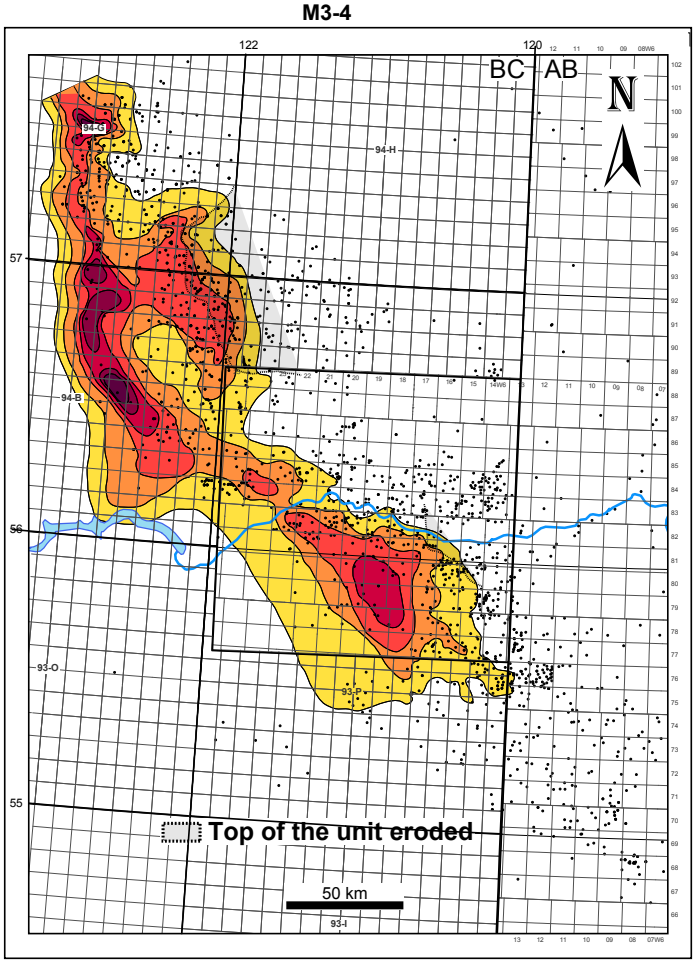

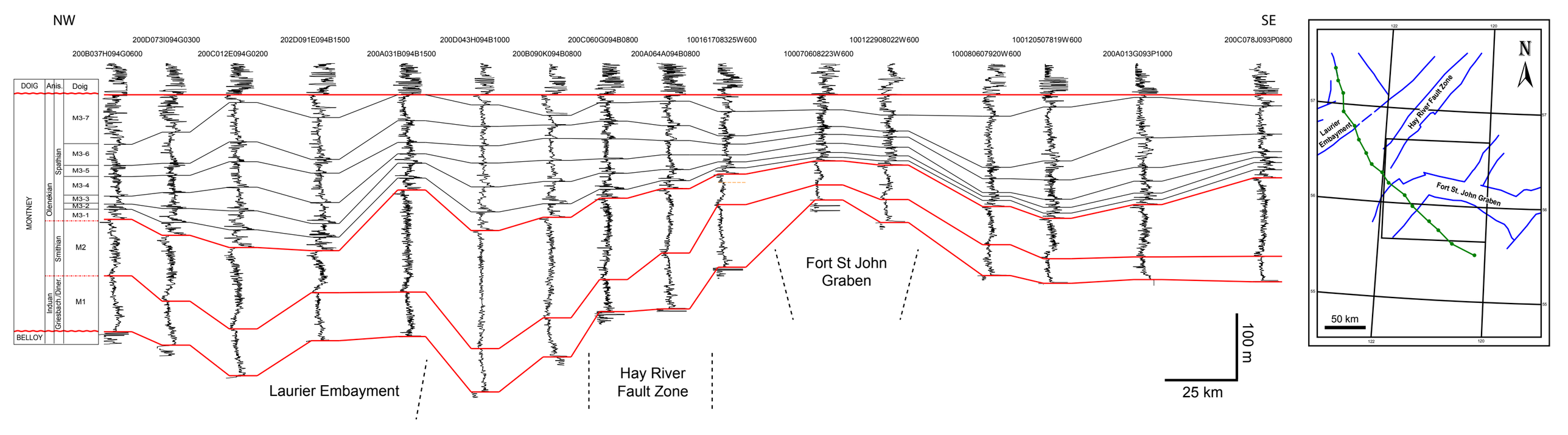
NW
SE
200D073I094G0300
202D091E094B1500
200D043H094B1000
200C060G094B0800
100161708325W600
100122908022W600
100120507819W600
200C078J093P0800
200B037H094G0600
200C012E094G0200
200A031B094B1500
200B090K094B0800
200A064A094B0800
100070608223W600
100080607920W600
200A013G093P1000
DOIG
Anis.
Doig
MONTNEY
Olenekian
Spathian
Smithian
Indian
Griesbach /Diner
M3-7
M3-6
M3-5
M3-4
M3-3
M3-2
M3-1
M2
M1
BELLOY
Laurier Embayment
Hay River Fault Zone
Fort St John Graben
100 m
25 km
N
Laurier Embayment
Hay River Fault Zone
Fort St. John Graben
50 km
122
120
57
56
55

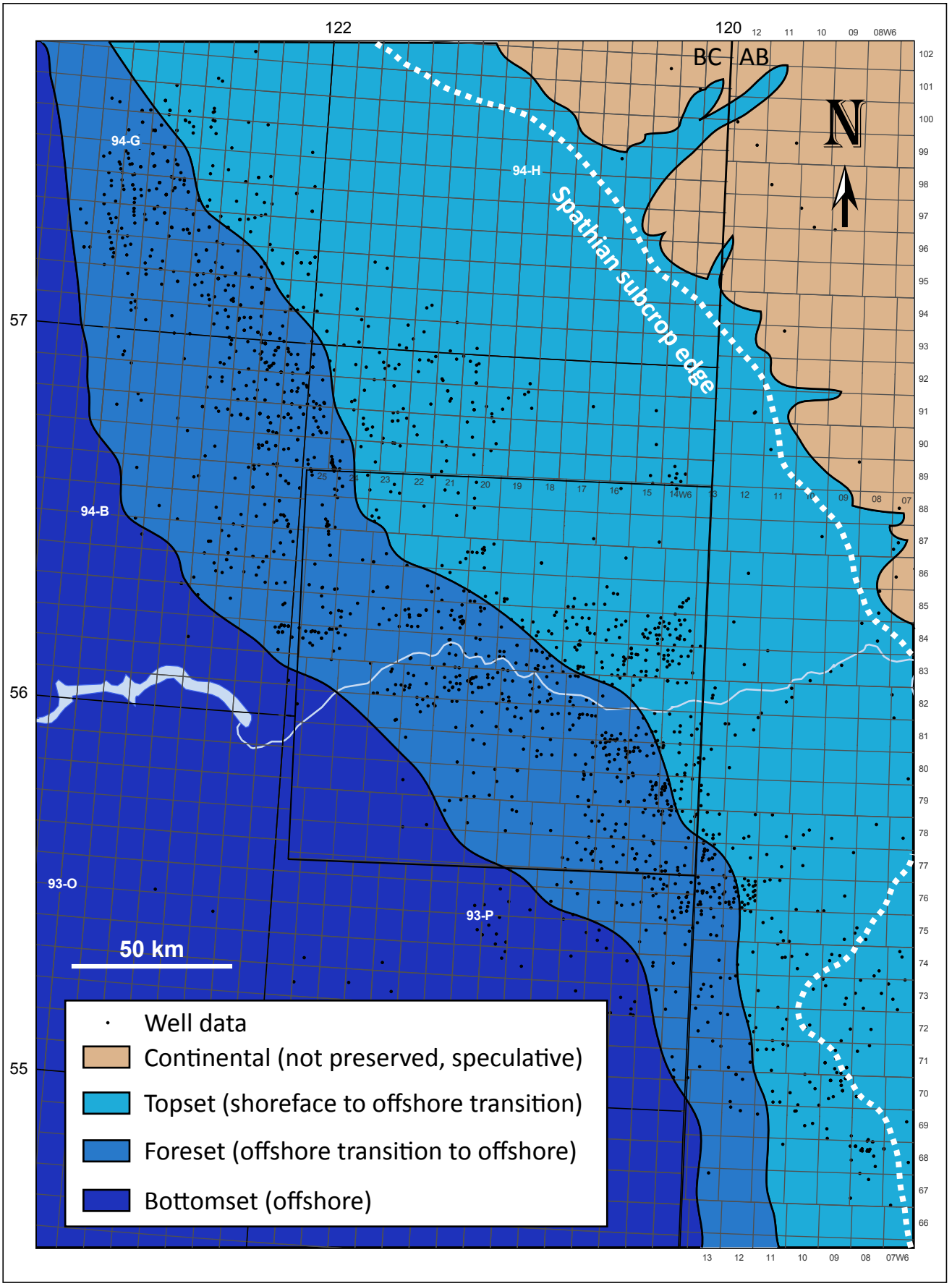
122
120
12 11 10 09 08W6
BC AB
N
94-G
94-H
Spathian subcrop edge
57
94-B
56
93-O
93-P
55
50 km
Well data
Continental (not preserved, speculative)
Topset (shoreface to offshore transition)
Foreset (offshore transition to offshore)
Bottomset (offshore)
13 12 11 10 09 08 07W6

Beg

Town

Altares

Groundbirch

Dawson

200 m

20 km

Smithian

Griesbachian-Dienerian

Spathian parasequence sets

M3-7

M3-6

M3-5

M3-4

M3-3

M3-2

M3-1

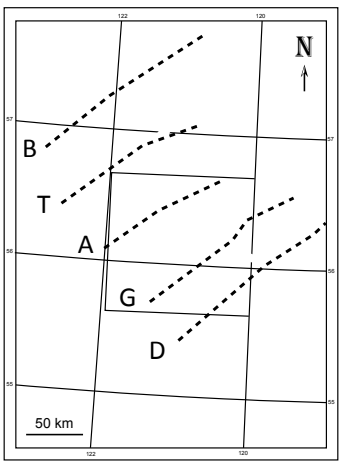

BC | AB

BC | AB